# Spin Fluctuation Resistivities of Fe-Ni-Zr Metallic Glasses

Srilakshmi V. Dantu

Department Of Physics, McGill University

A thesis submitted to the faculty of

Graduate Studies and Research in partial

fulfillment of the requirement for the

Degree of Master of Science

Department of Physics, McGill University

Montreal, Canada

October 1989

## ABSTRACT

The effect of spin fluctuations on the resistivities of 14 different $Fe_xNi_{1-x}Zr_2$ metallic glasses were analyzed in the temperature range from 4.2K to 80K. The corrections to the resistivity due to the superconductivity and quantum interference effects at very low temperatures were performed to obtain the spin fluctuation resistivity, $\rho_{sf}$, as a function of temperature and composition. It is found that, $\rho_{sf}$ varies as $T^2$ at very low temperatures, i.e. below around 20K, and as T at higher temperatures. This confirms the predictions of the two-band model of Kaiser and Doniach and the one-band model of Rivier and Zlatic. The spin fluctuation temperatures for all the compositions, were determined from both models. $T_{sf}$ calculated from the one-band model were about 30% higher than those calculated from the two-band model. The spin fluctuation temperature is lowest when the system is closest to the magnetic transition and it increases when the amount of magnetic species is reduced in the alloy, i.e. for x = 1, $T_{sf}$ = 10K (15K) and for x = 0.4, $T_{sf}$ = 64K (96K) for the two-band (one-band) model.

# RÉSUMÉ

L'effet des fluctuations de spin sur la résistivité dans 14 verres métalliques différents de $Fe_xNi_{1-x}Zr_2$ a été analysé dans la gamme de température allant de 4.2K à 80K. Les corrections à la résistivité dues à la supraconductivité et aux corrections quantiques, à très basses températures, ont été prises en compte de façon à obtenir la contribution des fluctuations de spin à la résistivité, $\rho_{sf}$, en fonction de la température et de la composition. On trouve que, $\rho_{sf}$ obéit une loi en $T^2$ à très basses températures, i.e T inférieures à 20K, et une loi en T pour les hautes températures. Ceci confirme les prédictions du modèle à deux bandes de Kaiser et Doniach et le modèle à une bande de Rivier et Zlatic. Les températures de fluctuations de spin pour toutes les compositions, ont été déterminées en utilisant les deux modèles. Les valeurs de $T_{sf}$ calculées à partir du modèle à une bande sont approximativement 30% supérieures à celles obtenues avec le modèle à deux bandes. La température de fluctuations de spin est basse quand le système est proche de la transition magnétique et augmente quand la proportion des espèces magnétiques est réduite dans l'alliage, i.e. pour x = 1, $T_{sf}$ = 10K (15K) et pour x = 0.4, $T_{sf}$ = 64K (96K) d'aprés le modèle à deux bandes (à une bande).

## ACKNOWLEDGEMENTS

I sincerely thank my supervisor, Prof. Zaven Altounian for his guidance, support and continuous encouragement during the course of this work. It is a great pleasure to work with him and I learned several things with his supervision.

My sincere thanks go to Sahnoune Abdelhadi for his many helpful suggestions. I would also like to thank all professors and students of the solid state group for the moral support and assistance.

I would especially like to thank my husband for constant encouragement. Finally, I thank Department of Physics, in particular, Prof. Altounian and his funding agency for the financial support during this work.

# Contents

# List of Figures

# List of Tables

# Chapter 1

# Introduction

Amorphous materials are quite similar to liquid metals in their general behaviour of the electrical resistivities. Both have generally high resistivities, $\rho$ and small temperature coefficient of resistivities, $\frac{1}{\rho}\frac{d\rho}{dT}$. Several theories were developed in order to understand the resistivity of amorphous metals at low as well as high temperatures [1]. In particular, the resistivity behaviour at low temparatures has been the most explored subject for the past decade. In disordered conductors, at very low temperatures, intense elastic scattering causes interference effects on the electron wavefunction, giving rise to quantum corrections to the conductivity known as weak localization [2] and enhanced electron-electron interaction [3]. In this temperature regime, the electron-electron interaction is dominant giving rise to $-\sqrt{T}$ temperature dependance of the resistivity. A large amount of theoretical [4] and experimental [5], [6] work has been done on this subject. Another low temperature phenomenon occuring in amorphous materials is superconductivity. In superconducting metallic

glasses, above and very close to the transition temperature, there is a contribution to the temperature dependent resistivity due to the superconducting fluctuations The influence of the superconducting fluctuations on $\rho(T)$ above the critical temperature was analyzed theoretically [7], [8] and [9] and experiments were carried out to test these theories [10], [11]. In brief, these phenomena occuring in amorphous materials at low temparatures is well studied.

There is also an anomalous resistivity behaviour that occurs in nearly magnetic amorphous systems. Although the transport properties of nearly magnetic amorphous systems are widely studied, very little is known about the anomalous resistivity behaviour that occurs in these systems. The first and only observation of this anomalous effect was seen recently by Strom-Olsen and co-workers [12], in the amorphous system, $Fe_xZr_{1-x}$ taking seven alloys from $Fe_{28}Zr_{72}$ through $Fe_{42.5}Zr_{57.5}$, which are on either side of the ferromagnetic transition [13] (see Figure 1.1). The anomalous effect was attributed to the presence of spin fluctuations. This phenomenon has been observed in the temperature dependence of the electrical resistivity of crystalline magnetic metals which have been studied for many years . In many instances, the resistivity is found to become nearly temperature independent at high temperatures compared to a characteristic temperature. As the temperature is decreased below the characteristic temperature, the resistivity is observed to decrease monotonically. At the lowest temperatures, the resistivity becomes proportional to $T^2$. For instance in 1964, Coles [14] discovered the remarkable temperature dependence of the resistivity of dilute RhFe alloys, containing 0.5 atomic% of Fe, in

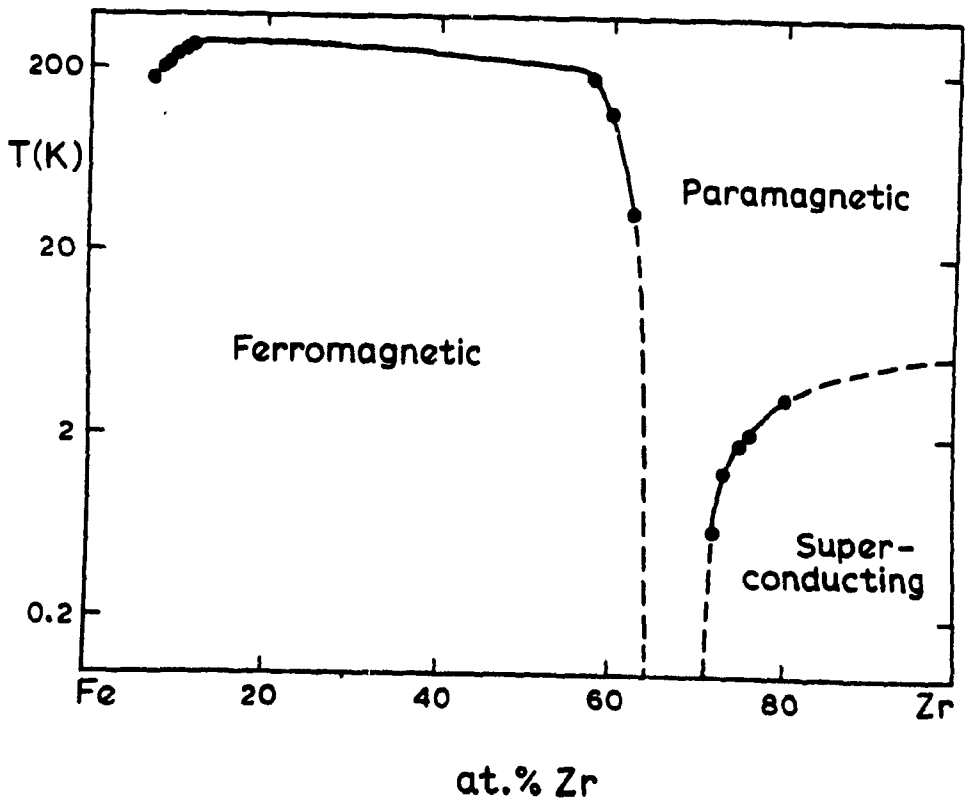


Figure 1.1: Magnetic phase diagram of Fe-Zr metallic glasses [13]

which after a very rapid linear increase with temperature, $\rho$ tends to flatten out into the shape of a knee at around 10K. Later, in 1968, Lederer and Mills [15] explained this type of behaviour, which was also found in many other transition metal alloys containing small amounts of magnetic (or nearly magnetic) impurities, as due to the scattering of conduction electrons from localized spin fluctuations.

The theories of spin fluctuations, have been demonstrated in a wide variety of nearly magnetic crystalline systems. The two band spin fluctuation model suggested by Kaiser and Doniach [16] appears applicable for the resistivities of the crystalline dilute PdNi alloys [17] and Rh-Ru-Fe alloys [18]. However, the measurements of Pauli susceptibility enhancement for Ir-Fe and Rh-Fe, [19], showed some disagreement with the spin fluctuation model suggested by Kaiser and Doniach, which predicts a large temperature dependence when the enhancement factor is large; whereas the experimental results in crystalline systems like Ir-Fe [20], seem to be in agreement with the one band model of Rivier and Zlatic [21]. Hence, further study of theoretical models in correspondance with experiments is required for quantitative understanding of the exerimental results.

The alloys studied in this thesis, were prepared by rapid quenching from the liquid state. The amorphous alloys prepared by this technique, are known as metallic glasses. Superconductivity in such metallic glasses was first reported in 1975 [22]. At present, a large number of metallic glasses are known to exhibit superconductivity and all of them are stable at room temperature. The most interesting feature, in all cases was that the transition temperatures of these glasses were found to be higher

than those of the corresponding bulk crystalline alloys. So far, not much work is done to incorporate spin fluctuations in understanding of superconductivity in metallic glasses. In order to have a quantitatively accurate calculation of superconducting transition temparature, it is necessary to include the influence of spin fluctuations. The behaviour of the Zr based metallic glasses illustrates very clearly the influence of spin fluctuations on superconductivity. This is directly evident from the data of [23]. At this point, it is important to look for independent evidence of spin fluctuations in these alloys perhaps via the field and temperature dependence of the resistivity. In our research, we analyse the effect of spin fluctuations on the temperature dependent resistivities of nearly magnetic metallic glass systems and carry out a critical evaluation of the one and two band theories.

Also, so far direct observations of the effects of spin fluctuations on the electrical resistivity of ternary metallic glasses has not been reported. In this thesis, we have analysed the effects of spin fluctuations in the resistivities of ternary metallic glass system $Fe_xNi_{1-x}Zr_2$. We examined the resistivites of these alloys in the temperature range from 4.2K to 80K. This is an ideal system to test spin fluctuation effects, since the sizes of Fe and Ni atoms are identical and the glassy alloys have similar structures. Thus the structure dependent contribution to the resistivity, $\rho_{str}(T)$ is assumed to be identical for all the alloys in the system. And since the binary $NiZr_2$ is farthest away from the magnetic transition, spin fluctuation effects are negligible, as shown by Batalla et al. [13]. On the other hand, in $FeZr_2$, which is closest to the magnetic transition composition, $Fe_{37}Zr_{63}$ [13], the contribution to

the temperature dependent resistivity from spin fluctuations $\rho_{sf}(T)$ is expected to be maximum. The temperature dependent resistivity of an alloy in this series can be written as:

$$\rho(T) = \rho_{str}(T) + \rho_{sf}(T) \tag{1.1}$$

For $NiZr_2$, $\rho_{sf}(T) = 0$

$$\rho^{NiZr_2}(T) = \rho_{str}(T) \tag{1.2}$$

Since, the resistivity due to the structure is assumed to be the same for all alloys in the series, $\rho(T)$ of an alloy can now be written as:

$$\rho^{alloy}(T) = \rho^{NiZr_2}(T) + \rho_{sf}{}^{alloy}(T) \tag{1.3}$$

Thus by subtracting off the resistivity of $NiZr_2$, we can obtain directly the spin fluctuation resistivity, $\rho_{sf}(T)$ for each alloy. The spin fluctuation resistivity obtained in this way is expected to be more accurate than that obtained by the procedure used in the previous experiments. For instance, in the work of Strom-Olsen and co-workers [12] on the binary $Fe_xZr_{1-x}$, two approximations were made. First, the spin fluctuation effects in $Fe_{28}Zr_{72}$ were assumed to be negligible. But, from the data of [13], it is clear that one can not neglect the spin fluctuation effect in $Fe_{28}Zr_{72}$. The second approximation is that a simple subtraction of $\rho^{alloy}$ from $\rho^{Fe_{28}Zr_{72}}$ would give $\rho_{sf}{}^{alloy}$. The variation of Zr content in the alloys, however, means that $\rho_{str}(T)$ is composition dependent. From the data of [24], the difference in $\rho_{str}(T)$ between $Fe_{42.5}Zr_{57.5}$ and $Fe_{28}Zr_{72}$, in the region of the resistivity anomaly, is estimated to be of the same order as $\rho_{sf}(T)$. In the present study, the selection of the alloy series eliminates the need for these approximations.

For superconducting alloys, in addition to the terms in equation 1.1, there will be another contribution from the superconducting fluctuations as mentioned earlier, which varies with the superconducting transition temperature. This contribution can be isolated, since the temperature dependence of the superconducting fluctuation resistivity is known. In addition, for all the alloys, at very low temperatures, the quantum corrections to the resistivity has to be accounted for. This procedure is also straightforward as the temperature dependence ($\rho \propto -\sqrt{T}$) is well established. The spin fluctuation resistivity can therefore be obtained directly and analyzed quantitatively to test various existing theories. Moreover, with our procedure, the critical or spin fluctuation temperature, $T_{sf}$, as well as the temperature dependence of $\rho_{sf}$ can be determined as a function of composition.

The thesis is organized in the following way: In the next chapter, an introduction to the theory of spin fluctuations suggested by Kaiser and Doniach is given and a brief introduction of the theory proposed by Rivier and Zlatic is also given. In the 3rd chapter the different experimental techniques used in this work are described. In the 4th chapter, the experimental results for the fourteen alloys are presented and discussed in the light of the above theories.

# Chapter 2

# Theoretical Background

It has been reported by many researchers e.g. [14], [25] that the resistivities of nearly ferromagnetic crystalline materials show an unusual behaviour with respect to temperature. In these crystalline systems such as RhFe, PdNi, IrFe etc. the resistivity due to magnetic impurities, shows a large decrease as the temperature decreases. Several authors [15], [16], [21], [26] have suggested models that attribute this behaviour to scattering of conduction electrons from localized spin fluctuations. Similar behaviour was seen for the first time in the Fe-Zr amorphous system [12]. To explain this anomalous behaviour in the amorphous system studied in this thesis, we will use a simple model of spin fluctuations suggested by Kaiser and Doniach [16] as well as the the one band model of Rivier and Zlatic [21].

## 2.1 Uniform And Localized Spin Fluctuations

Spin fluctuations in a ferromagnetic or nearly ferromagnetic metal can be explained as follows: In a ferromagnetic metal, spin fluctuations occur above its Curie point. We can think of these fluctuations as extensive regions in the metal in which the 'd' electrons are all polarized. This polarization in one region decays and appears spontaneously in other regions. Also, the interaction between 'd' electrons induce transient parallel spin alignment over those microscopic regions of the crystal and hence their magnetic susceptibility is enhanced relative to the Pauli susceptibility of a non-interacting electron gas. These fluctuations can also be expected to occur in nearly ferromagnetic metals. Spin fluctuations in a metal which is nearly ferromagnetic but still paramagnetic are sometimes referred to as "paramagnons". These are analogous to the density fluctuations in a fluid at temperatures close to but above the critical point of the fluid.

When dilute concentrations of ferromagnetic impurities are added to these systems, the spin fluctuations are enhanced in the vicinity of the impurity forming "local spin fluctuations", (LSF).

Spin fluctuation models mainly fall into two catogories: namely one band and two band models. The two band model of spin fluctuations proposed by Lederer and Mills [15], assumes that the heavy 'd' electrons provide the principal contribution to the magnetic properties of the metal and the lighter electrons provide the principal contribution to the conductivity. In this model it is shown that the time dependent

fluctuations of the magnetization at the site of a nearly magnetic transition metal impurity produce scattering of conduction electrons. This leads to a resistivity varying as $T^2$ at very low temperatures.

Kaiser and Doniach [16] extended the calculation of Lederer and Mills to higher temperatures. In this theory, the spin fluctuation resistivity varies as $T^2$ at sufficiently low temperatures, and slowly changes to T at temperatures of the order of 0.25 $T_{sf}$, where $T_{sf}$ is the spin fluctuation temperature, and $k_B T_{sf}$ is the energy of the peak in the localized spin fluctuation spectrum. If $T_{sf}$ is temperature dependent, then the model predicts a deviation from the linearity at higher temperatures due to the reduction of the enhanced susceptibility. It is reported by many researchers, that the changes in $T_{sf}$ are in fact consistent with changes in susceptibility enhancement.

In the one band model developed by Rivier and Zlatic [21], the difference in character between the electrons is neglected. The resistiviy behaviour predicted by this model, is qualitatively similar to that of the above two band models, i.e. both models predict $T^2$ and T behaviour of the spin fluctuation resistivity, but the main difference being the prediction of the high temperature fall-off of $\rho_{sf}$. Both models are appropriate when both impurity and host components are transition metals with similar electronic structure. In these systems, no localized virtual bound state is formed at the impurity and hence residual resistivity is relatively small. In other words, interference between potential scattering and spin fluctuation scattering is neglected in these models. These models, therefore, are appropriate for nearly-magnetic 3d impurities in 4d and 5d hosts from the same or nearby columns in the

periodic table. Thus, the temperature dependence of the resistivities of systems like Fe-Ni-Zr studied in this thesis, can be understood in terms of the strong localized spin fluctuations at the iron sites.

In the following sections we discuss the details of Kasier and Doniach's theory and present the model of Rivier and Zlatic.

## 2.2 Kaiser and Doniach Model

The scattering mechanism in most of the transitions metals can be understood by the two-band model of Mills and Lederer [27]. Kaiser and Doniach [16] used this model while taking each band as spherical. So, the parameters of the LSF (localized spin fluctuations) model are then assumed to be appropriate averages over the Fermi surfaces. When a dilute concentration of the transition metal impurities having similar electronic structure is added, the two band model is still assumed to be applicable but the main difference is that the d-band fluctuations are enhanced in the impurity cell. In this model, the mechanism by which the spin fluctuations affect the transport properties of the system is described by scattering of conduction electrons via the s-d exchange interaction, J. This scattering gives rise to a temperature dependent magnetic scattering component and is calculated using the Born approximation. The Coulomb repulsion, between the opposite spin electrons which is responsible for spin fluctuations, favours parallel alignment of the spin. These interactions cause enhancement of the susceptibility of a uniform electron band by

a factor

$$\alpha_0 = \frac{1}{1 - U\chi_0} \tag{2.1}$$

where $\chi_0$ is the susceptibility of the non interacting electron gas, and U is the intra-atomic exchange interaction. $\alpha_0$ evaluated at absolute zero is referred to as the Stoner enhancement factor. This enhancement clearly has important implications for the spin fluctuations in the metal since it profoundly affects the generalized susceptibility.

For dilute alloys containing impurities which are more nearly magnetic than the host, Lederer and Mills [15] derived the generalised susceptibility in the absence of a non-magnetic scattering potential

$$\chi_{alloy}(\vec{q}', \vec{q}, \omega) = \chi(\vec{q}, \omega)\delta_{\vec{k},\vec{k}'} + \frac{C\delta U \chi(\vec{q}, \omega)\chi(\vec{q}', \omega)}{1 - \delta U \bar{\chi}(\omega)} \tag{2.2}$$

Where C = impurity concentration, $\delta U$= the increase in intra-atomic exchange interaction in the impurity cell, $\bar{\chi}(\omega)$ is the host susceptability $\chi(\vec{q}, \omega)$ averaged over the wave vector,

$$\bar{\chi}(\omega) = \frac{1}{N}\sum_{q} \chi(\vec{q}, \omega) \tag{2.3}$$

The corresponding spectral density can be obtained by taking the imaginary part of the above equation, i.e.

$$A(\vec{q}, \omega) = 2Im\chi_{alloy}(\vec{q}', \vec{q}, \omega) \tag{2.4}$$

$$= 2Im\chi(\vec{q},\omega) + 2C\delta U Im\frac{\chi^2(\vec{q},\omega)}{1-\delta U\bar{\chi}(\omega)} \tag{2.5}$$

The second term is the spectral density of the localized spin fluctuations due to the impurities.

When the susceptibility enhancement at the impurity is much larger than that in the host, the specral density of the LSF, $\bar{A}(\omega)$, takes the universal shape [16].

$$\bar{A}(\omega) = \frac{a\hbar\omega}{\hbar^2\omega^2 + {k_B}^2{T_{sf}}^2} \tag{2.6}$$

Where $T_{sf}$ is the spin fluctuation temperature and the quantity 'a' is proportional to the enhancement factor for localized spin fluctuations.

Assuming that the conductivity arises from a single s-band, the electrical resistivity produced by inelastic collisions of conduction electrons with d-electron spin fluctuations can be calculated by the standard variational procedure applied to the Boltzmann equation as [16]:

$$\frac{\rho}{\rho_0} = \frac{\hbar}{k_B T}\int_0^\infty \frac{d\omega\omega\bar{A}(\omega)}{(e^{\beta\hbar\omega}-1)(1-e^{-\beta\hbar\omega})} \tag{2.7}$$

By using the spectral density given by the equation (2.6), the analytical expression for the spin fluctuation resistivity becomes [28]:

$$\frac{\rho_{sf}}{\rho_{s0}} = \frac{\pi T}{2T_{sf}} - \frac{1}{2} + \frac{T_{sf}}{4\pi T}\psi'(1+\frac{T_{sf}}{2\pi T}) \tag{2.8}$$

Where $\frac{\rho_{sf}}{\rho_{s0}}$ is the normalized resistivity due to localized spin fluctuations and $\psi'(x)$ is the trigamma function. The equation (2.8) is plotted in Figure 2.1. Now,

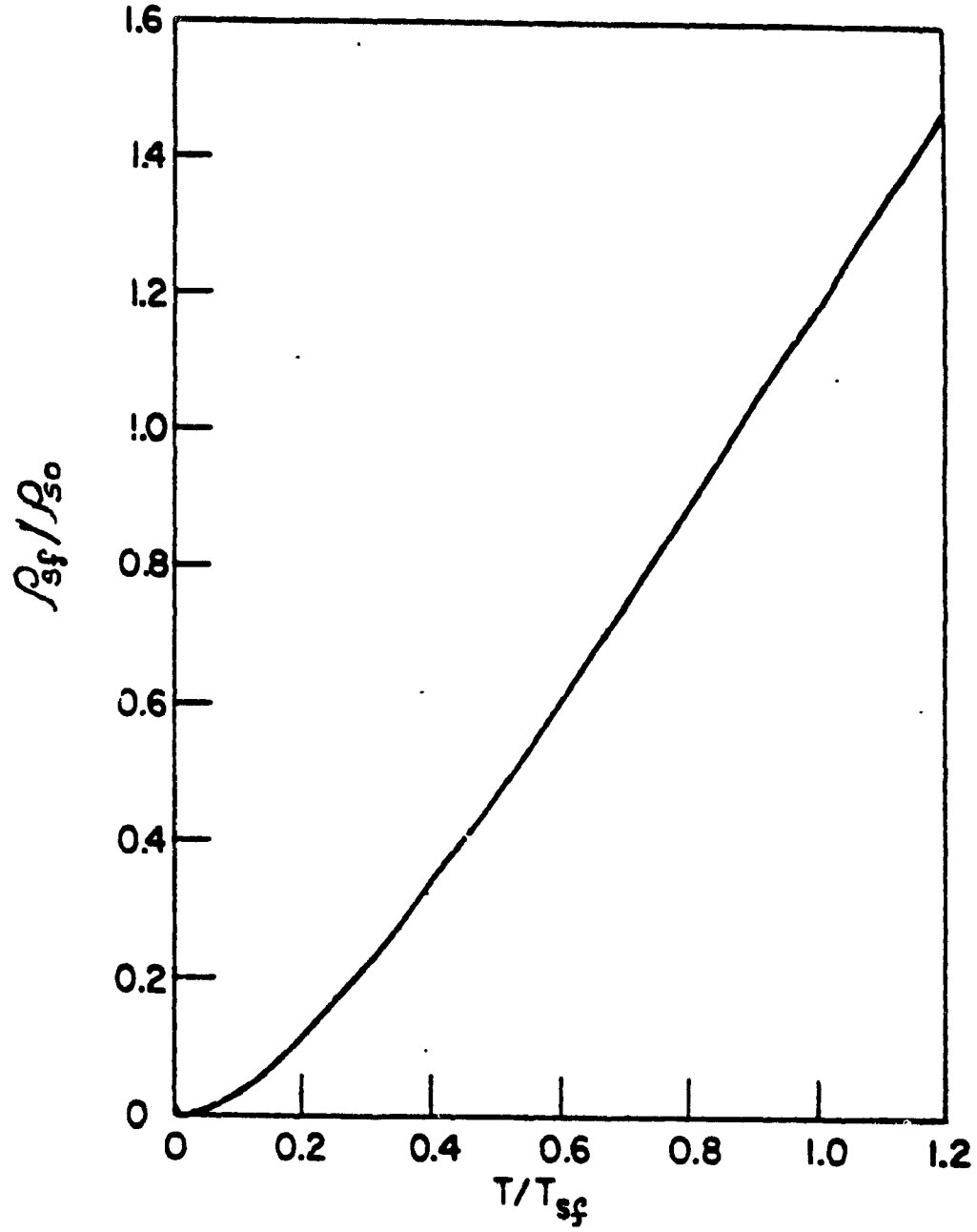


Figure 2.1: Universal curve for spin fluctuation resistivity in the two band model [28].

from this equation we can obtain expressions for $\rho_{sf}$ in the low and high temperature limits. From equation (2.8), when $T \rightarrow 0$,

$$\frac{\rho_{sf}}{\rho_{s0}} \approx \frac{\pi^2}{3}\left(\frac{T}{T_{sf}}\right)^2 \tag{2.9}$$

This is the low temperature behaviour found by Lederer and Mills [15] and also by Schindler and Rice [29]. When $T \rightarrow \infty$,

$$\frac{\rho_{sf}}{\rho_{s0}} \approx \frac{\pi}{2}\left(\frac{T}{T_{sf}}\right) - \frac{1}{2} \tag{2.10}$$

As we can see, there is a clear analogy between the universal curve for spin fluctuation resistivity obtained by Kaiser and Doniach, and the "Block-Gruneisen" expression for resistivity due to electron-phonon scattering, which also shows a linear T dependence at higher temperatures. This linear dependence on T is explained in terms of the Bose character of localized paramagnons. The number of thermal excitations is proportional to T. Thus the appearance of a linear law may be expected as a fairly general consequence of a low lying Bose excitation spectrum.

It was proposed that as T increases, the enhancement in the susceptibility decreases, causing the reduction in the resistivity below the linear law. According to the random phase approximation calculations, for

$$T \geq T_{sf} \tag{2.11}$$

$$\rho_{sf} \approx T\Delta\chi \tag{2.12}$$

Where $\Delta\chi$ is the susceptibility enhancement. Effect of the temperature dependence of local enhancement, $\alpha$, on $\rho_{sf}$, is shown in Figure 2.2 for different enhancement factors [16].

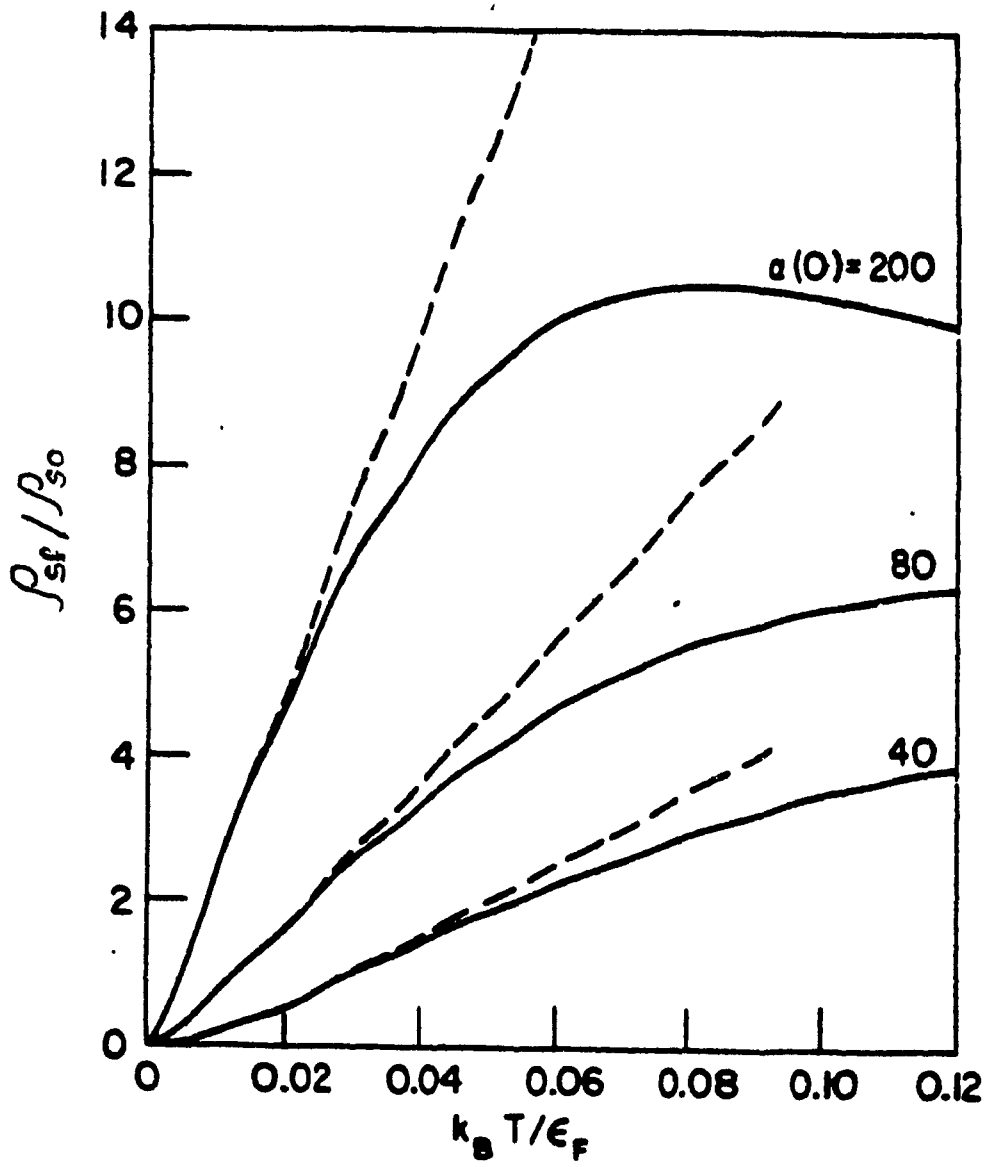


Figure 2.2: Effect of the temperature dependence of $\alpha(T)$ on spin fluctuation resistivity, for three different $\alpha(T)$ values. $\epsilon_F$ is the d-band energy at the Fermi level [16].

Thus the two-band model appears capable of accounting, though qualitatively, for the fall-off in the resistivity below the linear law at higher temperatures.

## 2.3 Rivier and Zlatic Model

Since in some metals, for example Rh and Ir, d-like electrons are thought to give a major contribution to the conductivity Rivier and Zlatic [21], [30] and [31] have suggested another method of calculating the effect of LSF on the transport properties.

In the model of Rivier and Zlatic [21], they start from an isotropic one-band Wolff model [25] in which the same electrons are responsible for magnetic properties and conductivity. Taking the spin fluctuations as confined to the impurity cell and the scattering as isotropic, the self energy of the d-like conduction electrons due to scattering by LSF and by a nonmagnetic potential V at the impurity site, was calculated. The t-matrix and transport properties were evaluated with no limitation on the strength of the coupling between conduction electrons and LSF. The effective scattering potential due to the LSF increases with increasing temperature following the thermal increase in the number of LSF, causing an increase in the scattering cross-section. An analytical expression for the resistivity of local spin fluctuations was obatined as

$$\frac{\rho_{sf}}{A} = 1 - [1 + \frac{\pi T}{T_{sf}} + \psi(\frac{1}{2} + \frac{T_{sf}}{2\pi T}) - \psi(1 + \frac{T_{sf}}{2\pi T})]^{-1} \qquad (2.13)$$

where $T_{sf}$ is the spin fluctuation temperature. $\psi(x)$ is the digamma function. A is a normalization constant taken so that $\rho_{sf} = 1$ at $T = \infty$.

The spin fluctuation resistivity is again a universal function of $T_{sf}$. In Figure 2.3, $\frac{\rho_{sf}}{A}$ is plotted against the reduced temperature $\frac{2\pi T}{T_{sf}}$. The resistivity increases with temperature yielding a curve, surprisingly similar to that given by Kaiser and Doniach's two band model. Here the fall off of the resistivity from the linear law is expected to occur around the spin fluctuation temperature. The temperature dependence of the resistivity can be divided into four main regions. The resistivity starts as $T^2$ at very low temperatures, where,

$$\frac{\rho_{sf}}{A} = \frac{1}{2}\pi^2[\frac{T}{T_{sf}}]^2 \tag{2.14}$$

(or)

$$\frac{\rho_{sf}}{A} = \frac{3\pi^2}{4}[\frac{T}{T_{sf}}]^2 \tag{2.15}$$

if the correction due to the Fermi window is included. At temperatures of the order of $0.9\frac{T_{sf}}{2\pi}$, the resistivity becomes linear, taking the value,

$$\frac{\rho_{sf}}{A} = 1.12\frac{T}{T_{sf}} - 0.7504 \tag{2.16}$$

Above the spin fluctuation temperature, the variation is logarithmic, where,

$$\frac{\rho_{sf}}{A} = C + B\log\frac{T}{T_{sf}} \tag{2.17}$$

Finally when $T \to \infty$, the spin fluctuation resistivity approaches the unitarity limit as:

$$\frac{\rho_{sf}}{A} = 1 - \frac{T_{sf}}{T} \tag{2.18}$$

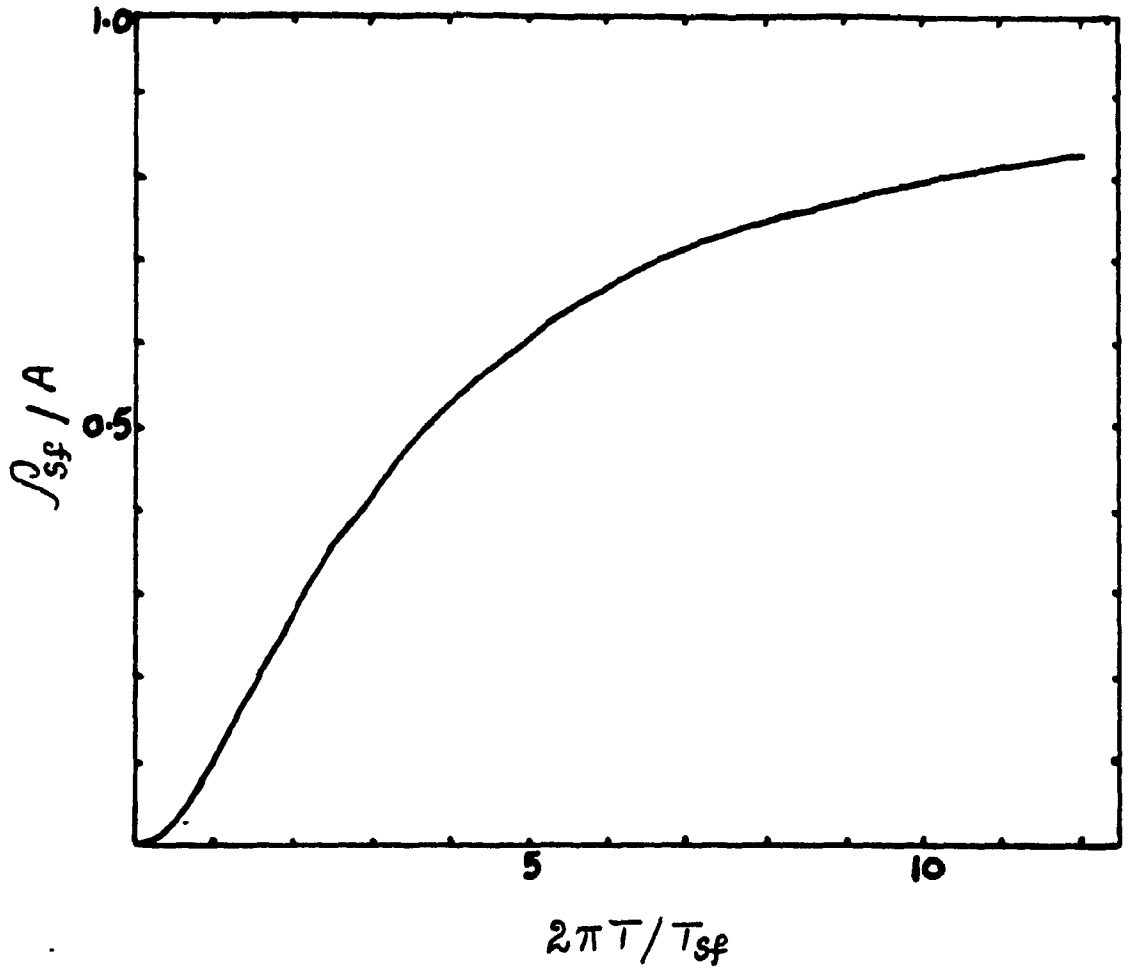


Figure 2.3: The normalized spin fluctuation resistivity as a function of the reduced temperature $\frac{2\pi T}{T_{sf}}$, from the one band model of [21].

In other words, we can think of this single band model as having impurity spins and conduction electrons coupled with an extremely large coupling constant J. The presence of the large coupling constant between them destroys their separate identities and implies a single band description of the alloy. For a large coupling constant J, the resistivity reaches the unitarity limit at high temperatures.

Thus the concave curvature of $\rho_{sf}$ to the T axis at higher temperature is due to the characteristic lnT dependence for scattering by a magnetic impurity and not to the temperature dependence of the LSF spectral density as assumed by Kaiser and Doniach, which is neglected in this model.

The similarity of the resistivity shapes in the one-band and two-band models indicates the general nature of the LSF resistivity shape.

## 2.4 Effect Of The Disorder On The Spin Fluctuation Spectrum

Recently, it was reported by Riseborough [32], that in many highly disordered paramagnetic materials, the spin fluctuation resistivity varies as $T^{\frac{3}{2}}$ rather than a $T^2$ . Since the introduction of impurities in a nearly magnetic system causes the impurity scattering to produce a loss of coherence in the spin fluctuation spectrum, he found that, by varying the impurity concentration, there is a correlation between the coefficient of the $T^{\frac{3}{2}}$ term and the magnitude of the residual resistivity. He used

a single hybrid band model, where the electron interaction is via a local Coulomb repulsion, to explain such behaviour.

## 2.5 Concluding Remarks

Thus both the one band and two band models predict the T and $T^2$ dependence of the spin fluctuation resistivity. In this thesis, we mainly concentrate on this low temperature regime. We would like to observe the variation of spin fluctuation temperature with concentration of the alloy. Since, in the system studied here, by varying the iron concentration in the alloy, we can significantly and directly vary the contribution of the spin fluctuations to the resistivity.

# Chapter 3

# Experimental Methods

In this chapter all the experimental details involved in this work are presented. First, sample preparation and different stages involved in it are described and then, a brief description of sample characterizatior is given. Finally, the experimental techniques for measuring the resistivities and the superconducting transition temperatures are described.

## 3.1 Raw Materials

The high purity raw materials needed for the preparation of alloys were purchased from the following suppliers :

Iron:

Alpha products ( Morton Thiokol products)

Danvers, MA, 01923, USA.

Purity : 99.99%

Morphology : lump.

Nickel:

Jonhson Matthey Chemicals limited,

Hertfordshire, England.

Purity : 99.999%

Morphology : 5 mm diameter rod.

Zirconium:

Jonhson Matthey Chemicals limited,

Hertfordshire, England.

Purity : 99.95%

Morphology : Crystal bar.

## 3.2 Preparation Of Samples

Apart from iron, all materials were etched to remove any surface contaminants. After etching, the materials were immediately immersed in distilled water to stop any further reaction and were finally cleaned with alcohol.

### 3.2.1 Arc - Melting

Appropriate amounts of the pure materials were weighed to within 0.005% of the desired alloy compositions. The appropriate constituents were then arc-melted under a titanium- gettered argon atmosphere. Fourteen ternary samples were made in the composition $Fe_xNi_{1-x}Zr_2$, x ranging from 0 to 1 (i.e. x=0, 0.1, 0.15, 0.2, 0.3, 0.33, 0.36, 0.4, 0.5, 0.6, 0.7, 0.8, 0.9, 1.0).

The resulting pellets were about 1.2 – 1.4g. These pellets were remelted several times under the same conditions to ensure homogeneity. If necessary, the samples were polished and cleaned with alcohol, between each melting, to remove any oxide layer. During the last melt, the samples were formed into ellipsoidal buttons. These buttons were then weighed a second time, and the mass loss in all cases was less than 0.1% from the original mass of the constituent elements.

### 3.2.2 Melt - Spinning

The amorphous ribbons were prepared by the melt-spinning technique. The melt-spinning apparatus is shown in Figure 3.1. This technique allows production of relatively large quantities of material with relative ease. In this technique, an alloy pellet is placed in a quartz crucible and is heated by an induction coil powered by LEPEL High Frequency RF-generator. The molten metal is ejected through the orifice at the bottom of the crucible onto the surface of a rapidly rotating copper wheel, which is well polished. The molten jet forms a thin ribbon on the wheel

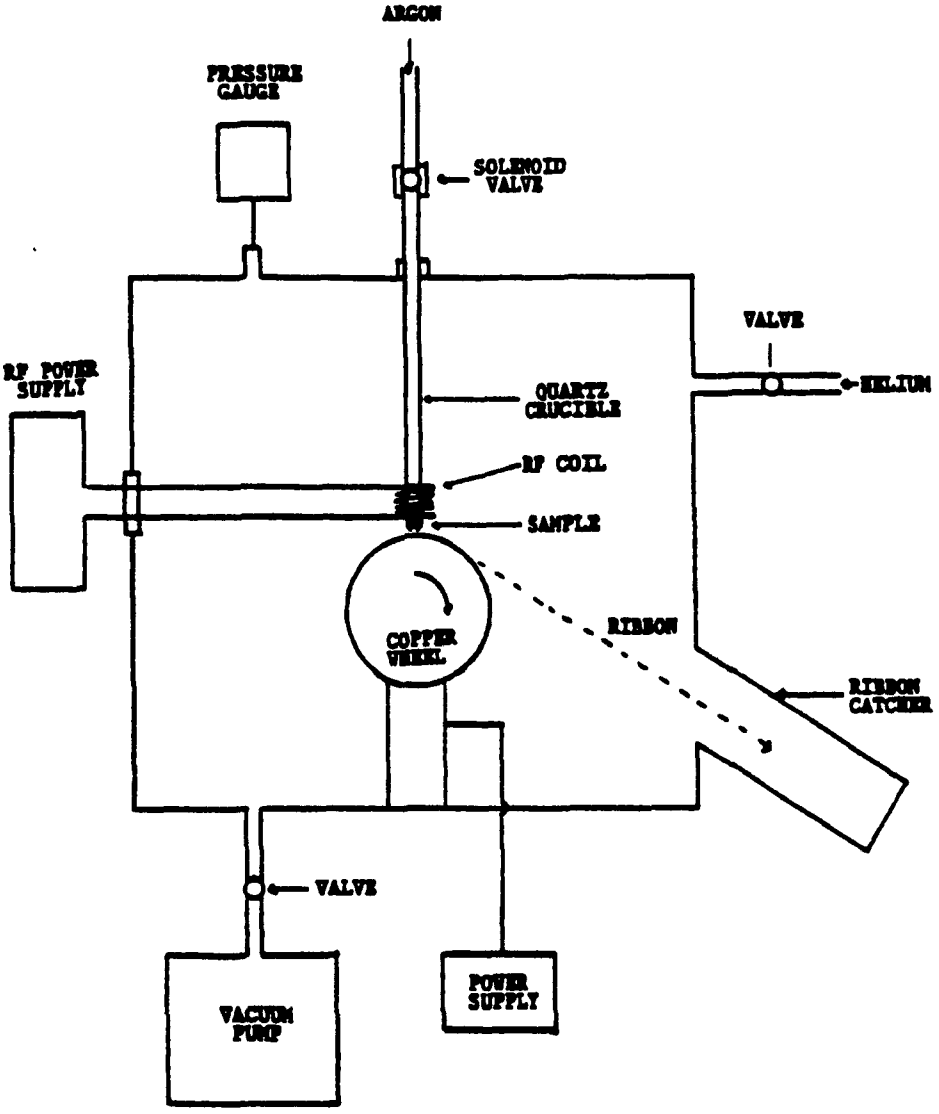


Figure 3.1: Schematic diagram of the melt spinning apparatus taken from [33]..

surface. To avoid oxidation effects, the melt-spinning was carried out under Helium atmosphere, at a pressure of about 35 kpa and high purity Argon was used for expulsion of the liquid ( at a pressure of about 100 kpa ). The tangential velocity of the wheel was kept at $58 \pm 5m/s$ throughout. The melt-spinning parameters, i.e. wheel speed, orifice diameter ($0.65 \pm 0.05mm$), and melt temperature were kept constant for making all the ribbons for all compositions. The resulting ribbons were typically 2mm wide and 20 – 25 $\mu m$ thick.

Throughout the preparation of the samples, care was taken to avoid oxygen contamination.

## 3.3 Sample Characterization

### 3.3.1 Verification Of The Amorphous Structure

The structural state of the samples was examined by X-ray diffraction using $CuK_\alpha$ radiation ($\lambda$ = 1.54056Å). A Nicolet-Stoe, automated powder diffractometer was used for this purpose. The diffracted beam passes through a graphite monochromator before entering the solid state detector, as shown in the Figure 3.2. For this particular diffractometer the sample was mounted on a flat piece of glass and was held in place by double sided sticky tape. The X-ray scans were done in the $2\theta$ range of 30 to 45 degrees, in 0.1 degree increments, and a counting time of 15 seconds at each position. All samples were judged to be satisfatory based on the absence of

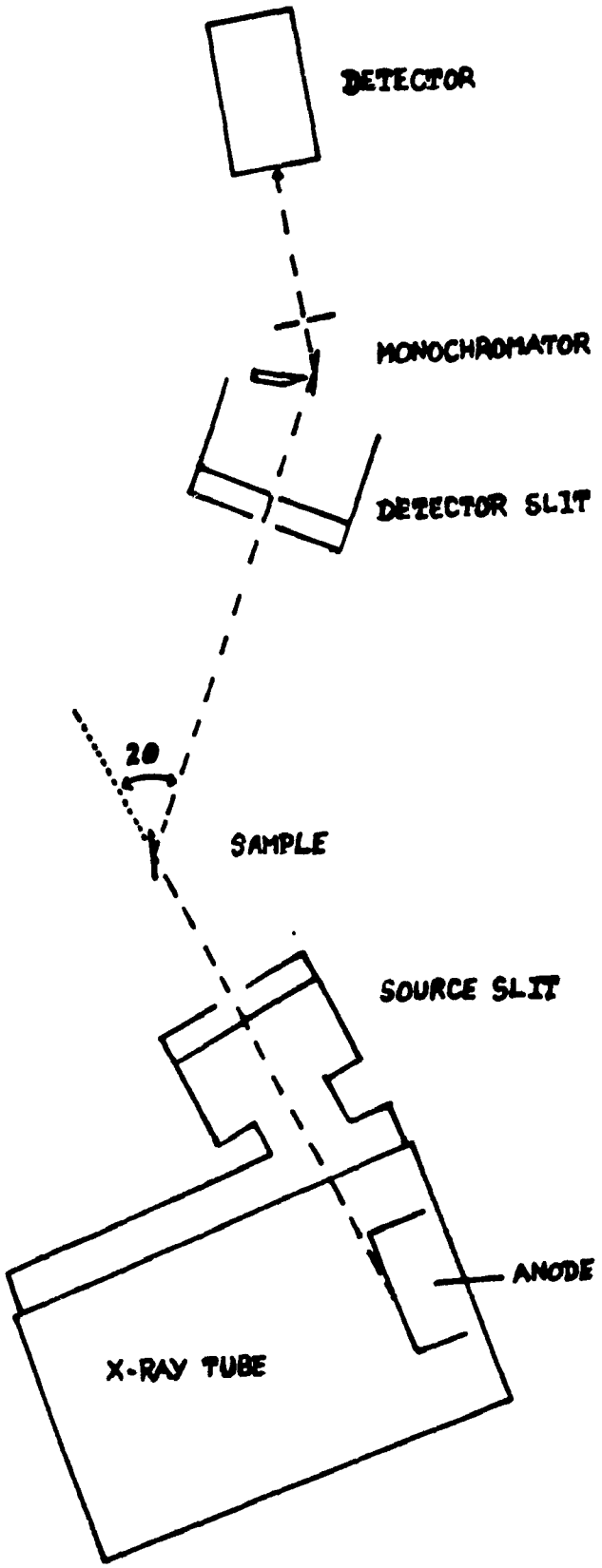


Figure 3.2: X-ray diffractometer

sharp diffraction peaks. Figure 3.3 shows an X-ray pattern typical of an amorphous sample. Nearest neighbour distance, NND, was calculated from the angle, $2\theta$, at which the maximum intensity of the reflected beam is observed, using Ehrenfest relation. It was found that NND was the same for all the compositions with in the experimental error of $8.10^{-3}$Å. For x = 0, NND was 3.005Å and for x = 1, NND was 2.990Å.

### 3.3.2 DSC Measurements

Differential Scanning Calorimetry (DSC) was used to determine the crystallization temperature of the samples. This can be determined from the peak positions of the crystallization exotherms. Enthalpy change ($\Delta H$) upon crystallization can be found by measuring the area under the exothermal peak in the DSC scan.

Figures 3.4 and 3.5 show typical DSC scans of four samples. Crystallization temperatures for different compositions varied from 665K to 678K at a heating rate of $10^{\circ}$/min.

### 3.3.3 Composition And Homogeneity

The composition and homogeneity of the samples were checked by electron-beam microprobe analysis. The sample which is to be analysed is irradiated with an electron beam of appropriate energy, which excites the electrons in the inner atomic shells. The excitations decay emitting X-rays of characteristic wavelength. The

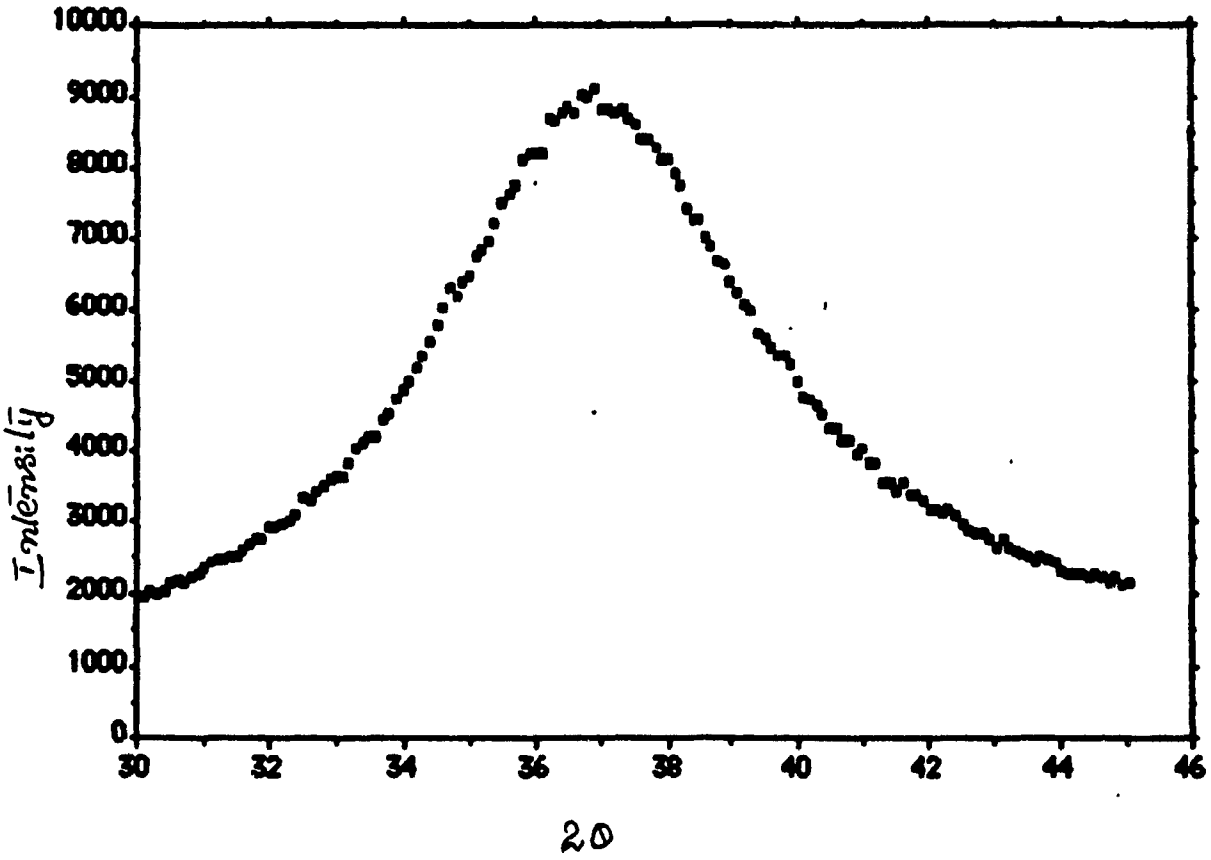


Figure 3.3: A typical X-ray diffraction pattern of an amorphous Fe-Ni-Zr alloy taken with $CuK_\alpha$ radiation

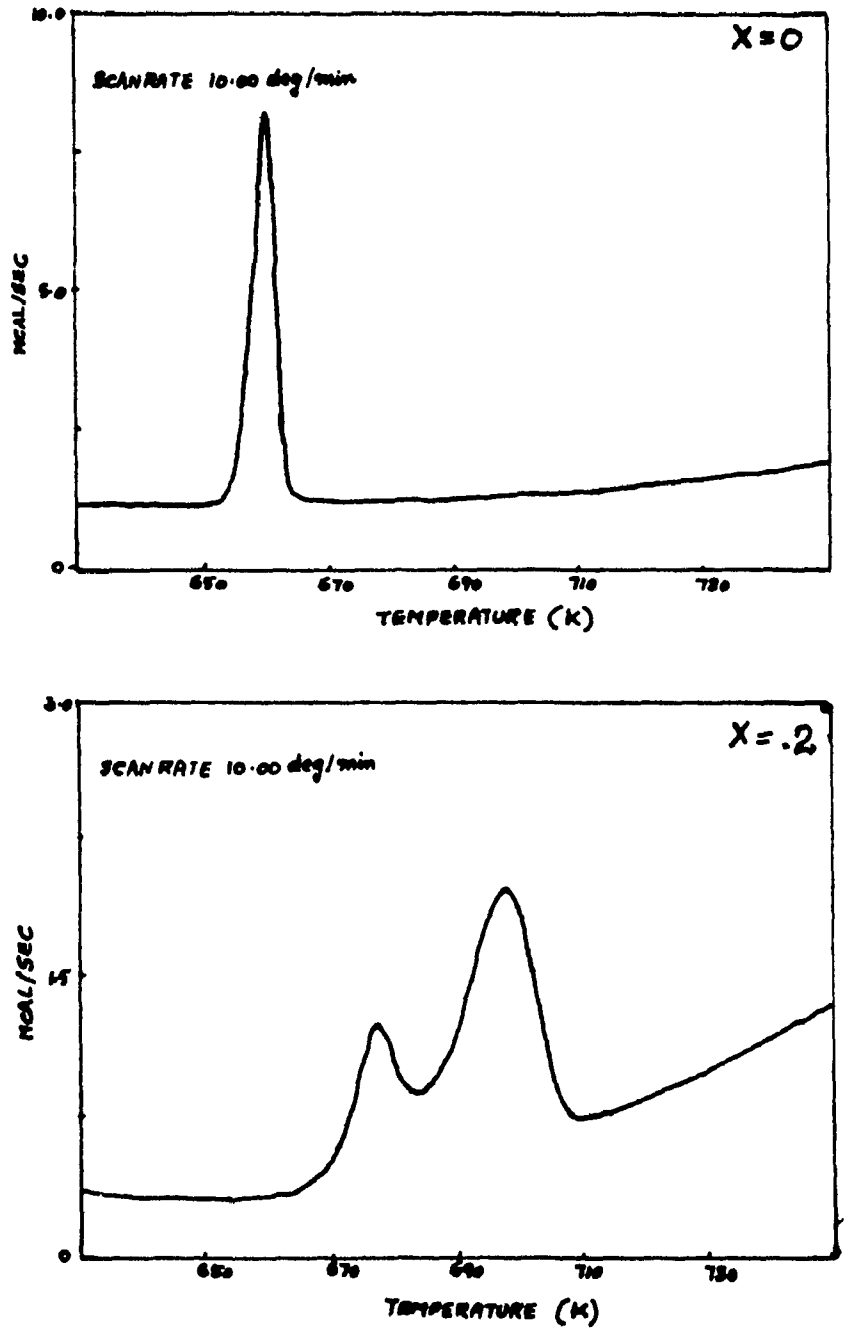


Figure 3.4: DSC scans of $NiZr_2$ and $Fe_{0.2}Ni_{0.8}Zr_2$.

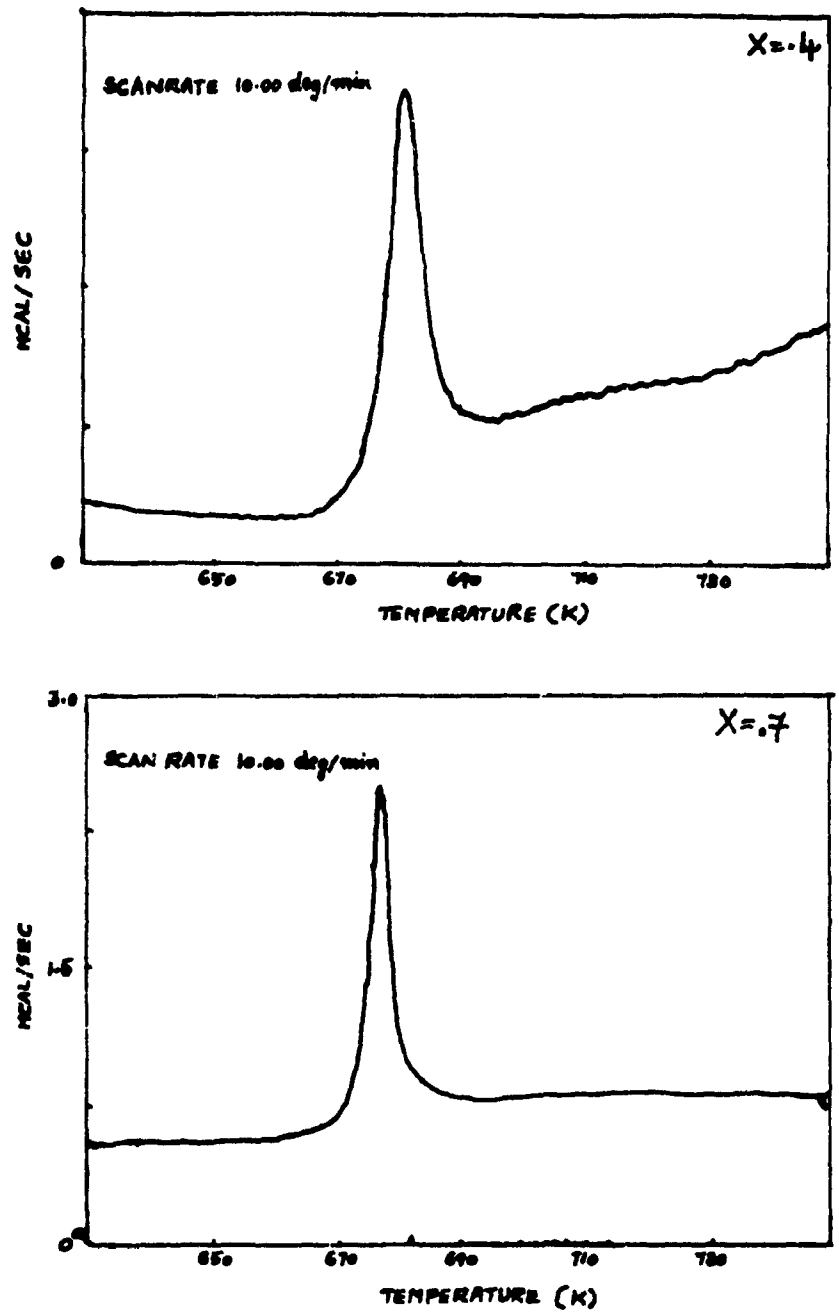


Figure 3.5: DSC scans of $Fe_{0.4}Ni_{0.6}Zr_2$ and $Fe_{0.7}Ni_{0.3}Zr_2$.

intensities of the X-rays are proportional to the concentration of the corresponding element. The analysis was done at different positions of the ribbon (sample). Listed in table 3.1 are the nominal and measured compositions for all the samples. The analysis shows that the samples are homogeneous over the whole length. For all the alloys, except $Fe_{0.8}Ni_{0.2}Zr_2$, the concentration of each constituent differs by less than 2% from the expected nominal composition.The accuracy of the instrument is quoted at 0.2 atomic% for the elements investigated.

## 3.4 Room Temperature Resistivity Measurements

Electrical resistance at room temperature was measured using a 4-probe dc technique, on a sample of $\approx$ 1 metre length with a Keithley #172A multimeter. Care was taken to make good current and voltage contacts.

The density values of the samples needed to convert resistance to resistivity were determined using Archimedes' method with toluene as the liquid medium. The mass in air ($w_{air}$) and in toluene ($w_{toluene}$) was measured using a mechanical balance (Mettler H20T). Toluene was used because of its low surface tension. The density of the sample is given by

$$d_{sample} = \frac{W_{air}}{W_{air} - W_{toluene}} d_{toluene} \tag{3.1}$$

where $d_{toluene}$ is the density of toluene which is $0.8669 g/cm^3$ at 20C.

The density of the samples varies linearly with the Fe content. After determining the density, the cross-sectional area A of the sample can be calculated by

| *Nominal composition (atomic%)* | *Detected composition (atomic%)* | | |
|---|---|---|---|
| | Fe | Ni | Zr |
| $Fe_{33.3}Zr_{66.7}$ | 32.9 | 0 | 67.1 |
| $Fe_{30}Ni_3Zr_{66.7}$ | 30.5 | 3.4 | 66.0 |
| $Fe_{26.7}Ni_{6.7}Zr_{66.7}$ | 25.7 | 6.3 | 68.0 |
| $Fe_{23.3}Ni_{10}Zr_{66.7}$ | 24.3 | 9.9 | 65.8 |
| $Fe_{20}Ni_{13.3}Zr_{66.7}$ | 20.7 | 13.2 | 66.15 |
| $Fe_{16.7}Ni_{16.7}Zr_{66.7}$ | 17.2 | 16.7 | 66.1 |
| $Fe_{13.3}Ni_{20}Zr_{66.7}$ | 14.0 | 20 | 66.0 |
| $Fe_{12}Ni_{21.3}Zr_{66.7}$ | 12.5 | 21.5 | 66 |
| $Fe_{11}Ni_{22.3}Zr_{66.7}$ | 11.6 | 22.4 | 66.0 |
| $Fe_{10}Ni_{23.3}Zr_{66.7}$ | 10.3 | 23.5 | 66.3 |
| $Fe_6Ni_{26.7}Zr_{66.7}$ | 6.9 | 26.8 | 66.3 |
| $Fe_5Ni_{28.3}Zr_{66.7}$ | 5.2 | 28.8 | 66.0 |
| $Fe_{3.3}Ni_{30}Zr_{66.7}$ | 3.6 | 30.4 | 66.0 |
| $Ni_{33.3}Zr_{66.7}$ | 0 | 33.6 | 66.3 |

Table 3.1: Electron-beam microprobe results

the relation,

$$A = \frac{m}{l.d} \tag{3.2}$$

The room temperature resistivity of the sample is then, given by

$$\rho = \frac{RA}{l} = \frac{Rm}{l^2 d} \tag{3.3}$$

where $R$ is the sample resistance, $l$ is the length of the ribbon, $d$ is the density and $m$ is the mass of the sample. The error in the resistance measurement was estimated to be = 0.1 ohm, and that of mass is $\delta m = 10^{-4} g$. The error in the density mmeasurements was estimated to be $\delta d = 0.04 g/cm^3$.

In Figure 3.6, the composition versus the room temperature resistivity of different samples is plotted. Within these errors, it can be clearly seen that the room temperature resistivity is independent of the composition, x.

Finally, the values shown here are in good agreement on both ends with those of [24], [34]. In table 3.2, densities and room temperature resistivities for all the alloys are given.

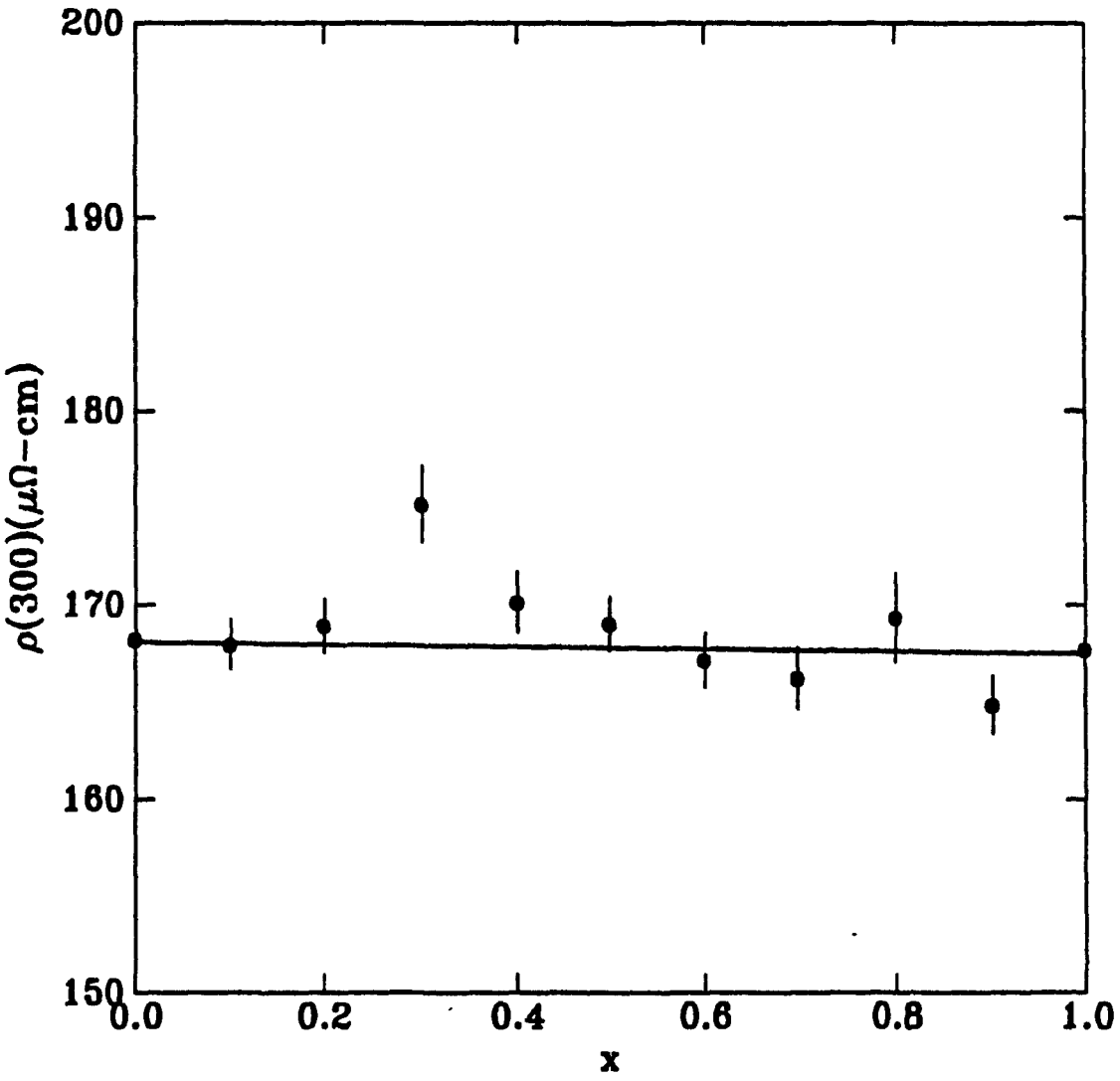


Figure 3.6: Room temperature resistivity of $Fe_xNi_{1-x}Zr_2$ metallic glasses

| Composition | $d\ (g/cm^3)$ | $\rho\ (\mu\Omega - cm)\ \pm\delta\rho$ |
|---|---|---|
| $FeZr_2$ | 6.92 | 167.7 ±1.5 |
| $Fe_{0.9}Ni_{0.1}Zr_2$ | 6.93 | 164.8 ±1.5 |
| $Fe_{0.8}Ni_{0.2}Zr_2$ | 6.94 | 169.3 ±2.3 |
| $Fe_{0.7}Ni_{0.3}Zr_2$ | 6.96 | 166.2 ±1.6 |
| $Fe_{0.6}Ni_{0.4}Zr_2$ | 6.97 | 167.1 ±1.4 |
| $Fe_{0.5}Ni_{0.5}Zr_2$ | 6.99 | 169.0 ±1.4 |
| $Fe_{0.4}Ni_{0.6}Zr_2$ | 7.00 | 170.1 ±1.6 |
| $Fe_{0.36}Ni_{0.64}Zr_2$ | 7.00 | - |
| $Fe_{0.33}Ni_{0.67}Zr_2$ | 7.01 | - |
| $Fe_{0.3}Ni_{0.7}Zr_2$ | 7.01 | 175.1 ±2.0 |
| $Fe_{0.2}Ni_{0.8}Zr_2$ | 7.03 | 168.9 ±1.4 |
| $Fe_{0.1}Ni_{0.9}Zr_2$ | 7.04 | 167.9 ±1.3 |
| $NiZr_2$ | 7.06 | 168.2 ±1.8 |

Table 3.2: Mass density and room temperature resistivity.

## 3.5 Measurements of Temperature Dependence of Resistivity and Superconducting Transition Temperature

A sensitive four-terminal a.c resistance bridge designed by Muir, Strom-Olsen, Cochrane and Kastner [35], [36] was used to measure small changes in the resistance of the sample with temperature.

A detailed circuit diagram of the apparatus is shown in Figure 3.7. The circuit operates in the following way: Two identical transformers $T_1$ and $T_2$ supply equal currents to both sample and reference loops. Transformer $T_3$ eliminates current imbalances to first order. Using an ITHACO 391A lock-in amplifier, the difference between the voltage across the sample and voltage across the inductive voltage divider were measured. A small quadrature signal given by the small difference in the resistance of the two loops or capacitive coupling across the transformers, was monitered with a second lock-in amplifier and adjusted to zero during the measurements.

The output voltage of the lock-in amplifier was calibrated by changing the reference voltage across the inductive voltage divider, which is proportional to a calibrated resistance change $\Delta R$, and reading the corresponding output voltage change $\Delta V$, at a constant temperature. The sample resistance is given by

$$R_{sample} = R_{reference} + \frac{\Delta R}{\Delta V} V_{lock-in} \tag{3.4}$$

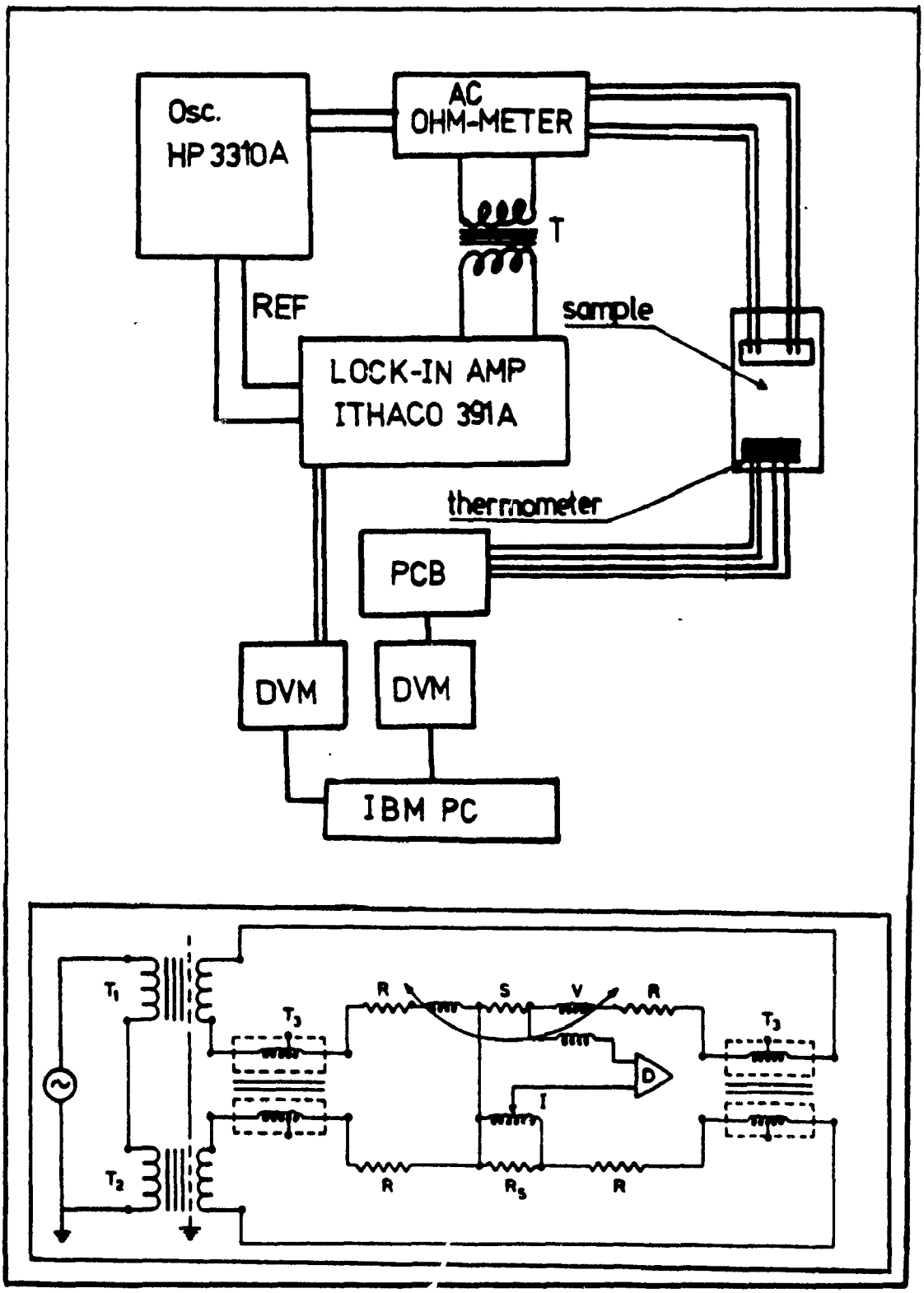


Figure 3.7: Schematic diagram of the a.c resistance bridge and data aquisition system. Inset- circuit diagram of the a.c resistance bridge, taken from [36]

where $R_{reference}$ is the reference resistance and $\frac{\Delta R}{\Delta V}$ is the calibration constant. $V_{lock-in}$ is the lock-in amplifier output voltage which is read by a Keithley #175A digital multimeter.

The noise on the output voltage of the bridge was reduced using a time constant of 1 to 3 seconds. With this technique a change of $10^{-5}$ in a 1 ohm resistor can be easily detected.

The sample holder used in these measurements is shown in the Figure 3.8. The copper sample holder block is held in position by four thin walled stainless steel tubes, which contain copper leads for the necessary electrical connections. Two samples of 2 cm long ribbons were mounted, one on each side of the mylar coated copper block using G. E. Varnish. The thin mylar film acts as an electrical insulator between sample and the copper block. Voltage and current contacts were made with conductive silver paint. Care was taken to make very good contacts to reduce noise. A calibrated Carbon glass resistance thermometer (Lake Shore Cryotronics CGR - 1 - 500) was used to measure the temperature of the sample. Accuracy of the thermometer varies from 0.1% at 1.5K to ±0.05% at 300K. Conductance of the thermometer was monitored by a conductance bridge (SHE Corporation model PCB 843 - 8). The temperature dependence of the resistance was measured from 4.2K to 80K. The sample chamber was first evacuated to a pressure of approximately 50 millibars. Then the sample temperature was increased by controlling the current in the heater wire wrapped around the copper block as shown in Figure 3.8. In these measurements, the changes in the sample resistance and its temperature were read

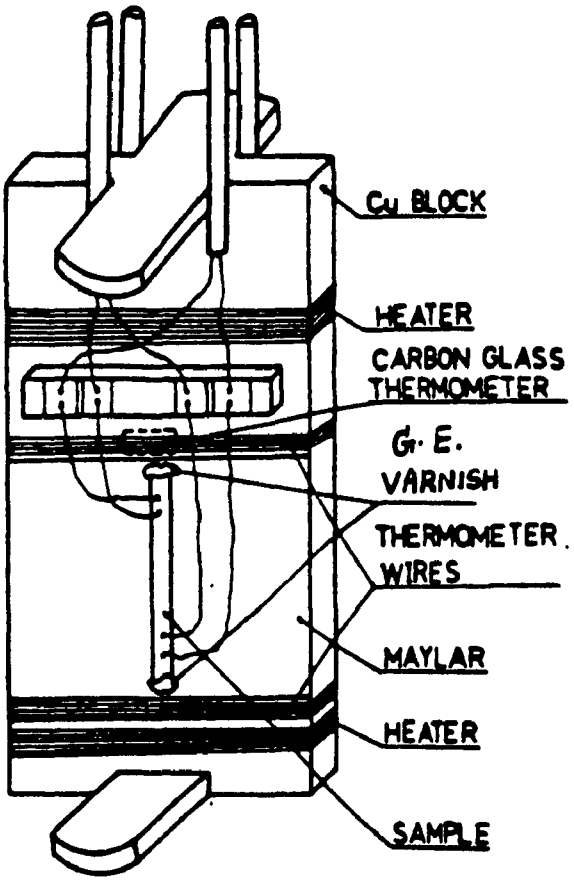


Figure 3.8: Diagram of the resistance probe sample holder used for resistivity and superconducting transition temperature measurements

by two Keithley #175A digital multimeters. All the data were stored in an IBM personal computer and were transferred to a SUN work station for further analysis.

For the measurements of the superconducting transition temperatures, the sample was first immersed in liquid He. Then, by reducing the He pressure in the sample chamber, the temperature of the bath was lowered from 4.2K to 1.5K, and the changes in the sample resistance were monitored throughout.

# Chapter 4

# Results and Discussion

In the first section the experimental measurements of the temperature dependent resistivities for Fe-Ni-Zr metallic glasses ($Fe_xNi_{1-x}Zr_2$, x=0 to 1) are presented and discussed. In the second and third sections, we review the quantum corrections to the conductivity in metallic glasses at low temperatures, and the contribution of superconducting fluctuations to the resistivity respectively. Finally we show how we extract the spin fluctuation resistivity and the results are compared to the predictions of the Kaiser and Doniach and Rivier and Zlatic theories of spin fluctuations.

## 4.1 Temperature Dependent Resistivities of Fe-Ni-Zr Metallic Glasses

The alloys studied are $Fe_xNi_{1-x}Zr_2$, x ranging from 0 to 1. The resistivities of the alloys are plotted in Figure 4.1 relative to their value at 4.2K, over the temperature range 4.2K to 80K. In the electrical resistivities of these glasses two striking features are observed :

1. The magnitude of the room temperature resistivity within experimental uncertainities, is independent of the Fe concentration as shown in Figure 3.6.

2. The temperature dependence of the resistivity, however, is a strong function of the Fe concentration.(see Figure 4.1)

Upon the addition of Fe, a striking positive anomaly emerges leading to a maximum in $\rho(T)$ before the curve resumes a monotonic decrease with temperature. The magnitude of the anomaly increases with increasing Fe content, and becomes maximum for $FeZr_2$ alloy. This is similar to the behaviour seen in some systems in crystalline and in amorphous alloys, mentioned earlier in chapter(2) and can be understood by the scattering of conduction electrons from spin fluctuations.

There are basically two main contributions to the temperature dependent resistivities of these alloys. One is the resistivity component due to the disorder of the alloy. This contribution is assumed to be the same for all the alloys in the series (It is shown in chapter 3 that the resistivity, at room temperature and NND are independent of composition). The second contribution to the temperature depen-

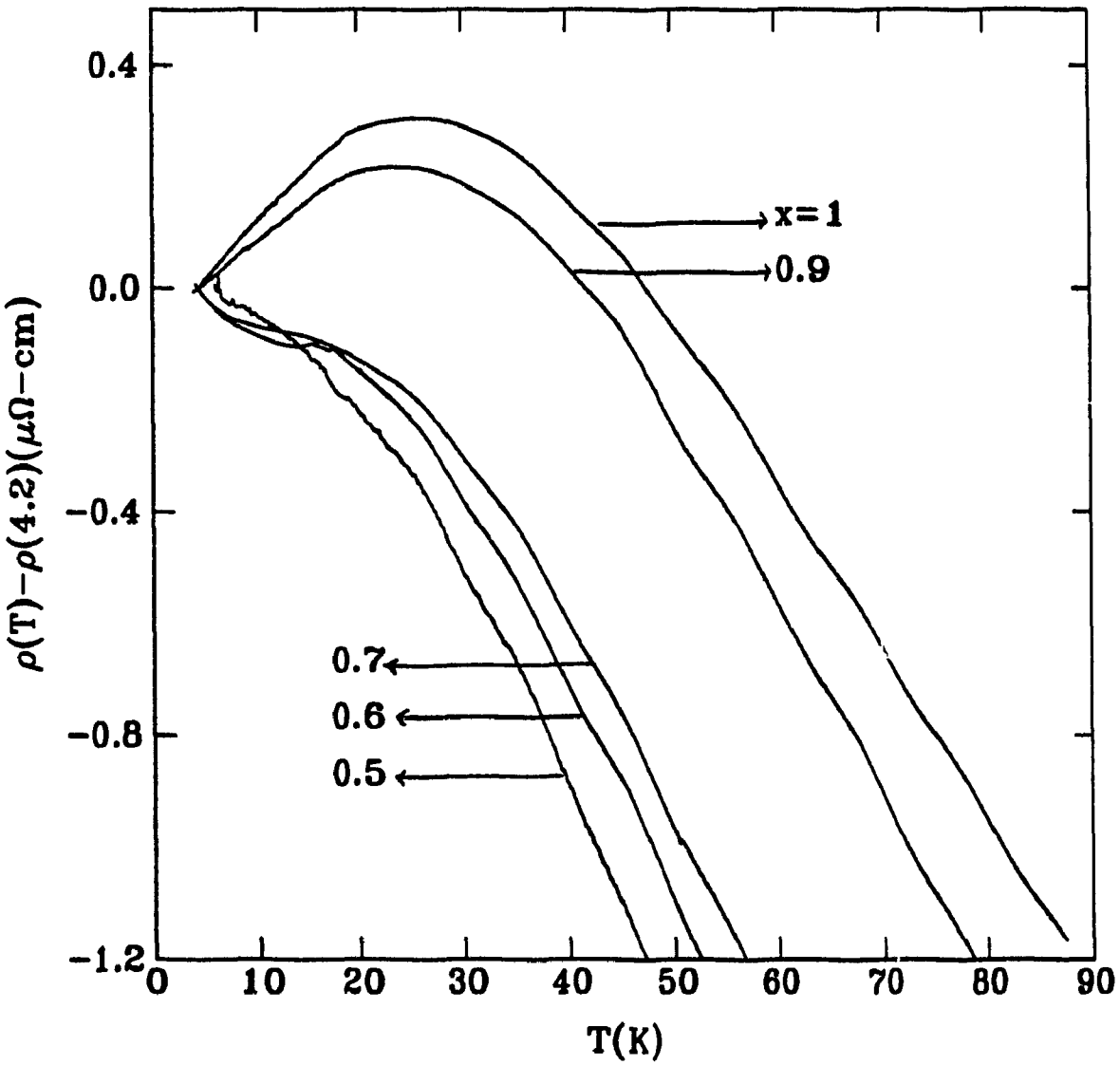


Figure 4.1: Resistivities of $Fe_xNi_{1-x}Zr_2$ metallic glasses as a function of temperature. Some of the alloys are not shown here to avoid overlapping of the curves.

dent resistivity comes from the spin fluctuations discussed in chapter 2, and this component is different for different alloys in the series: it increases with increasing Fe content as the system approaches the magnetic transition. For $NiZr_2$ the temperature dependent resistivity comes from the disorder scattering only, since its composition is farthest away from the magnetic transition; i.e. the contribution from spin fluctuations is zero. As mentioned in the introduction, the behaviour of $NiZr_2$ is representative of the resistivity due to disorder, therefore the resistivity contribution from the spin fluctuations in the ternary alloys may be obtained, in principle, by simply subtracting off the resistivity of $NiZr_2$ .

In addition to these contributions, at low temperatures, the quantum corrections to the resistivity have to be taken care of. Some of the alloys, however, are also superconducting at low temperatures . So, to obtain the contribution to the resistivity from spin fluctuations at low temperatures, we first have to subtract the resistivity component due to superconducting fluctuations. Since their superconducting transition temperatures are low, these corrections due to superconductivity and quantum corrections are necessary only below 15K. The resistivity components due to spin fluctuations are then obtained by subtracting the resistivity of $NiZr_2$. In this way $\rho_{sf}$, can be analysed in the entire temperature range from 4K to 80K by fitting the experimental curves, to the expression of Kaiser and Doniach or Rivier and Zlatic.

## 4.2 Quantum Corrections to the Conductivity

Recent experiments have shown that the electrical conductivity, $\sigma$, of a large number of metallic glasses varies as $-\sqrt{T}$ at very low temperatures [37]. When the temperature is increased this behaviour slowly changes to T. From the lowest temperatures available to about 20K, this $\sqrt{T}$ dependance is observed in different metallic glass systems.

This behaviour is indicative of quantum effects, implying that corrections to the usual semiclassical treatment of conduction in metallic glasses are necessary. There are mainly two sources of quantum corrections: weak localization [2] and enhanced electron-electron interaction [3]. Both of these corrections are important when the electronic mean free path becomes short so that electron propagation between scattering events is no longer free electron like but diffusive [2].

The weak localization takes account of the effects resulting from the significant interference between scattered partial waves. In disordered conductors, at low temperatures, the coherent interference between the conduction electron wave functions scattered around complementary paths by the defects of the system, causes weak localization effect. The elastic scattering time of the conduction electrons at low temperatures can exceed the inelastic scattering time by several orders of magnitude. As a result, a conduction electron can be scattered by the impurities from one state to another state without loosing its phase coherence. In these conditions, a coherent superposition of the scattered electron waves occurs which results in an

enhanced probability of back-scattering of the electron wave [Bergman] [5], which in turn causes an increase in the resistivity of the conductor.

The correction to the resistivity arising from the weak localization is given by [38]:

$$\frac{\Delta\rho(T)}{\rho^2(4.2)} = \frac{e^2}{2\pi^2\hbar}[3\sqrt{\frac{1}{D\tau_{s0}} + \frac{1}{4D\tau_i}} - \sqrt{\frac{1}{4D\tau_i}}] \tag{4.1}$$

where D = diffusion constant, $\tau_{s0}$ = spin-orbit scattering time, and $\tau_i$ = electron-phonon scattering time. Approximately one finds due to weak localization [39],

$$\Delta\rho \propto -T \tag{4.2}$$

The second phenomenon, the interaction effect is a consequence of an increase in the strength of the electron-electron interaction when electrons diffuse fast through the alloys, which is a direct consequence of the disorder. Due to the diffusive motion of the electrons, the screening of the Coulomb potential of the electron by other electrons is reduced, causing a strong interaction between the conduction electrons. In this case the resistivity of the conductor is increased, similar to weak localization. This phenomenon is sensitive to inelastic, spin-orbit, spin scattering and to the presence of magnetic fields.

The correction to the resistivity arising from the enhanced electron-electron interaction in the case of superconductors, is given by [3] and [37]:

$$\frac{\Delta\rho}{\rho_{4.2}} = -\frac{0.915e^2\rho_{4.2}}{4\pi^2\hbar}[\frac{4}{3} - \frac{3}{2}F^* - \frac{2}{\log\frac{T_c}{T}}][\frac{k_BT}{D\hbar}]^{\frac{1}{2}} \tag{4.3}$$

where $F^* = F - \lambda$. F = screening parameter, $\lambda$ = electron-phonon mass enhancement parameter, $T_c$ = superconducting transition temperature and D is the diffusion constant. In the case of non-superconductors, $T_c$ is replaced by the Fermi temperature, $T_F$.

At low temperatures, $\rho \propto -\sqrt{T}$ seen in many amorphous metals, suggests that the electron-electron interaction is dominant in determining the low temperature behaviour of the resistivity. Indeed in Y-Al [40], Strom Olsen and coworkers found that, below 4K the contribution from weak localization is negligible and the temperature dependence from the enhanced electron-electron interaction contribution is dominant. Similar results were obtained in many other metallic glasses [6], [41] and [42]. Figure 4.2 shows the low temperature resistivity of $Ca_{70}Al_{30}$ (taken from [6]).

In our alloy series, $Fe_{0.6}Ni_{0.4}Zr_2$ can be taken as the representative of the quantum interference effects at low temperatures, since, for this alloy, the superconducting transition temperature is far below 0.5K and it is far away from the magnetic transition composition. Its resistivity varies as $-A\sqrt{T} + B$ from 7K down to 4K, which can be seen in Figure 4.3.

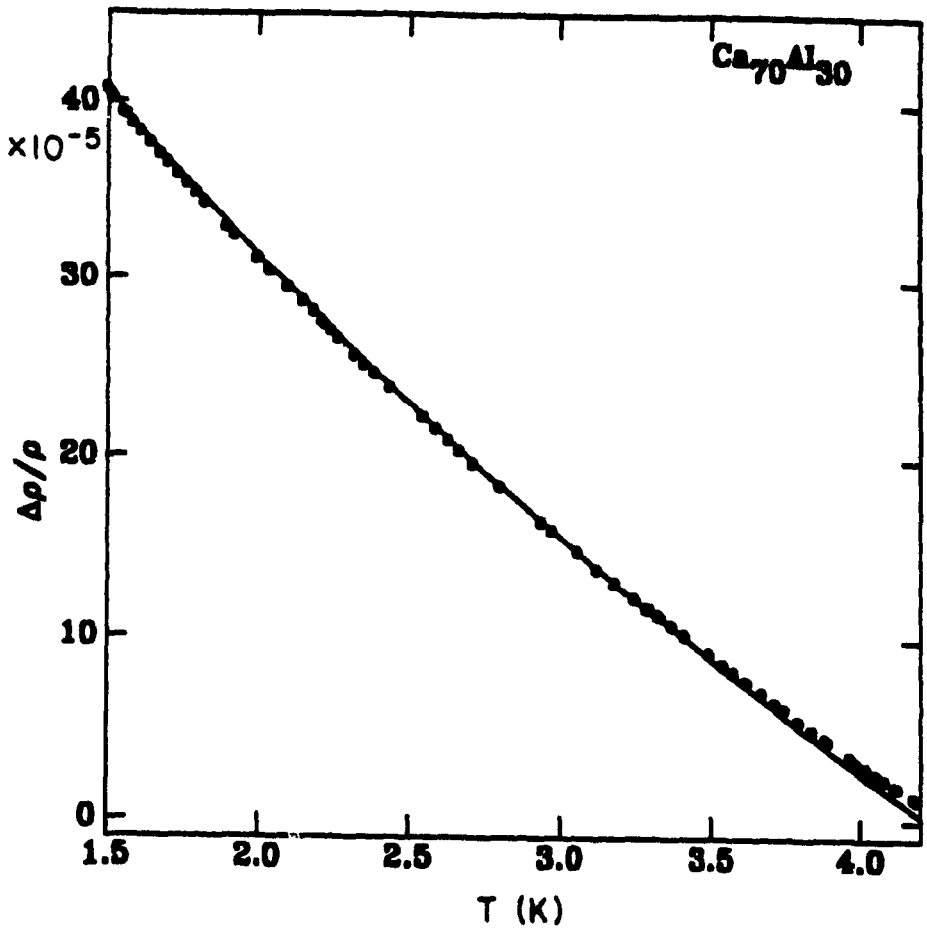


Figure 4.2: Low temperature resistivity of $Ca_{70}Al_{30}$, solid line is the fit according to equation 4.3.

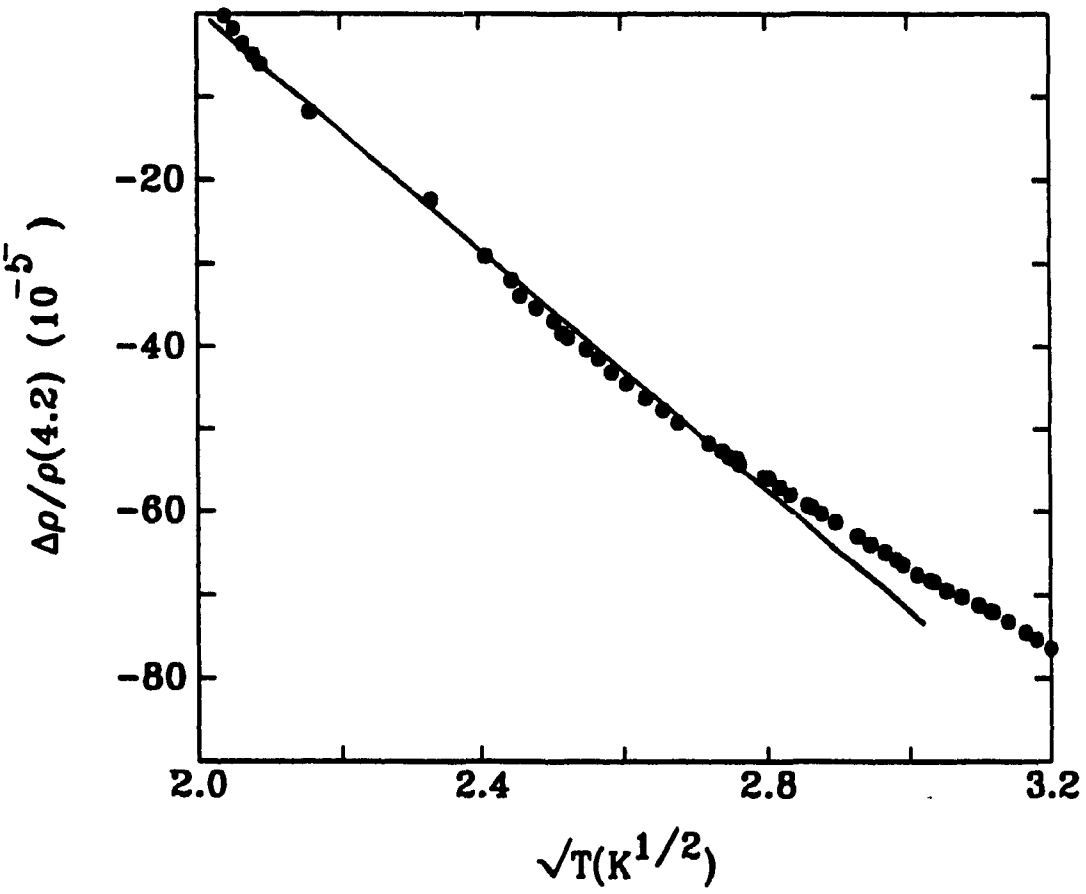


Figure 4.3: Normalized resistivity of $Fe_{0.6}Ni_{0.4}Zr_2$ plotted as a function of square root of the temperature.

## 4.3 Resistivity Component due to Superconducting Fluctuations

Since some of the alloys in this series are superconducting, the superconducting transition temperatures ($T_c$) of the different samples were measured. The superconducting transitions for different alloys are shown in Figure 4.4. The width of the transition as indicated by the difference between the temperatures at which the resistance was 10% and 90% of its normal state value, for different alloys are given in table 4.1. The width of the transition in all the alloys is less than 30 mK, indicating a very sharp transition, and is indicative of a homogeneous alloy. Figure 4.5 shows the variation of $T_c$ with the Fe content in the alloys. From the figure it is very clear that $T_c$ decreases with increasing Fe content.

In these disordered superconductors, in particular for the Ni- rich alloys, the contribution to the temperature dependent resistivity arising from the superconducting fluctuations above the transition temperature must be accounted for. In contrast to ordered superconductors, superconducting fluctuations, i.e. Cooper pairs with a small correlation length and a short life time, can exist in disordered superconductors far above the transition temperature $T_c$. There are basically two types of contributions to the resistivity, one from the current carried by the superconducting fluctuations known as the Aslamasov - Larkin term [8] and another from the scattering of normal electrons by the superconducting fluctuations, which is known as the Maki - Thomson term [8].

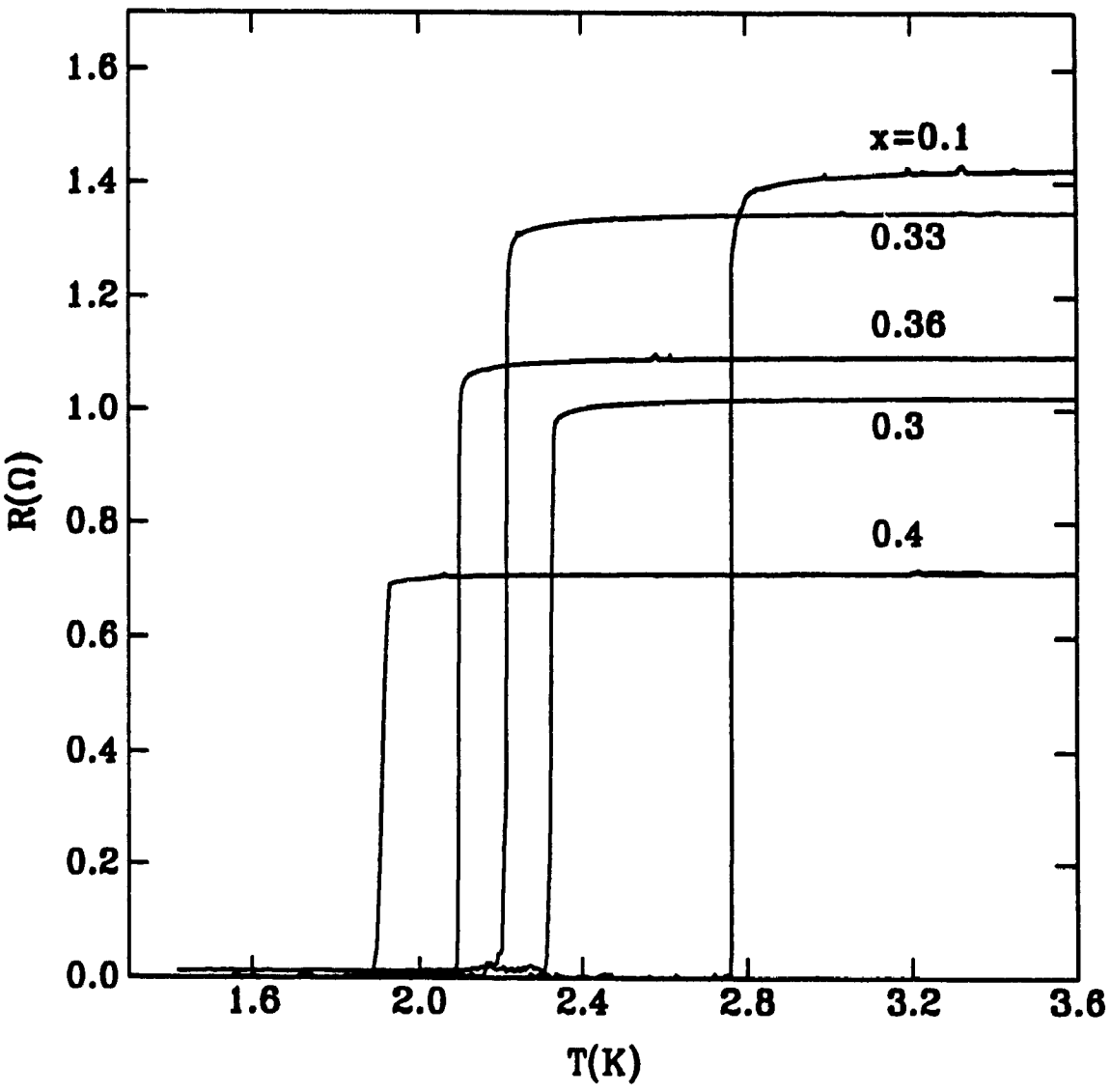


Figure 4.4: Resistance as a function of temperature for five $Fe_xNi_{1-x}Zr_2$ metallic glasses, showing the superconducting transition.

| *Composition* | $T_c$ (K) | *Transition width (mK)* |
|---|---|---|
| $Fe_{0.4}Ni_{0.6}Zr_2$ | 1.9 | 26 |
| $Fe_{0.36}Ni_{0.64}Zr_2$ | 2.096 | 9 |
| $Fe_{0.33}Ni_{0.67}Zr_2$ | 2.213 | 15 |
| $Fe_{0.3}Ni_{0.7}Zr_2$ | 2.32 | 14 |
| $Fe_{0.1}Ni_{0.9}Zr_2$ | 2.76 | 9 |
| $NiZr_2$ | 2.8 | 6 |

Table 4.1: Superconducting transition temperatures and transition widths.

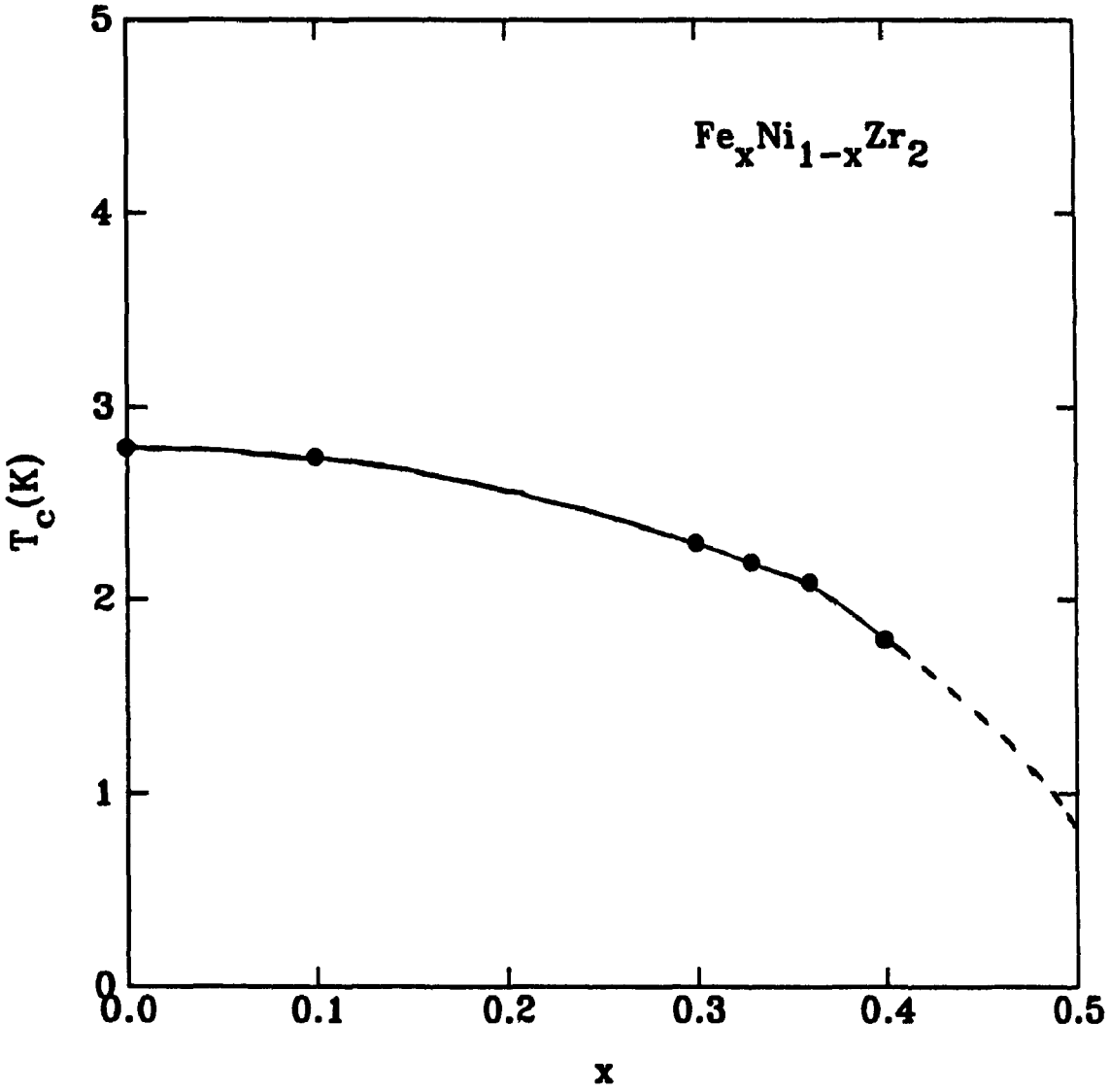


Figure 4.5: Variation of $T_c$ with the Fe content (x) in the alloy for $Fe_xNi_{1-x}Zr_2$ metallic glasses

Ami and Maki [8] have shown that the Aslamasov - Larkin contribution decreases rapidly above the transition temperature. This is in agreement with the experimental results of Johnson and coworkers [10], who also reported that it is negligible above $1.3T_c$. Johnson et al. showed that the theoretical predictions of the Aslamasov-Larkin theory provide a good quantitative account of the data near $T_c$. The apparent breakdown of the theory can be interpreted as resulting from the breakdown of the Ginzberg Landau free-energy function. In contrast, the Maki-Thomson term persists to well above $T_c$. As shown by Ami and Maki, it consists of two parts: one with a large magnetic field and small temperature dependance; and a second with a small field and drastic temperature dependance.

Johnson et.al. [10] found in amorphous metallic systems such as $La_{75}Au_{15}Cu_{10}$ and $Mo_{30}Re_{70}$, that this temperature dependent fluctuation conductivity decays as $exp(-\gamma\sqrt{t})$. Where$\sqrt{t}$ is the order parameter of the superconducting transition,

$$t = \frac{T - T_c}{T_c} \tag{4.4}$$

and $\gamma$ is a measure of the free energy difference between the normal and superconducting state. They reported that the quantity, $\gamma$, is constant in all of the their samples studied (i.e. $\gamma = 4.5$) . A plot of $\log(\frac{\Delta\sigma_{ac}}{\sigma_0})$ against $\sqrt{t}$ of the experimental result is reproduced here in Figure 4.6.

Fe-Ni-Zr metallic glasses studied in this thesis, differ in their fluctuation induced conductivity because of their different transition temperatures. But, since their physical parameters are approximately the same, a similar result is expected

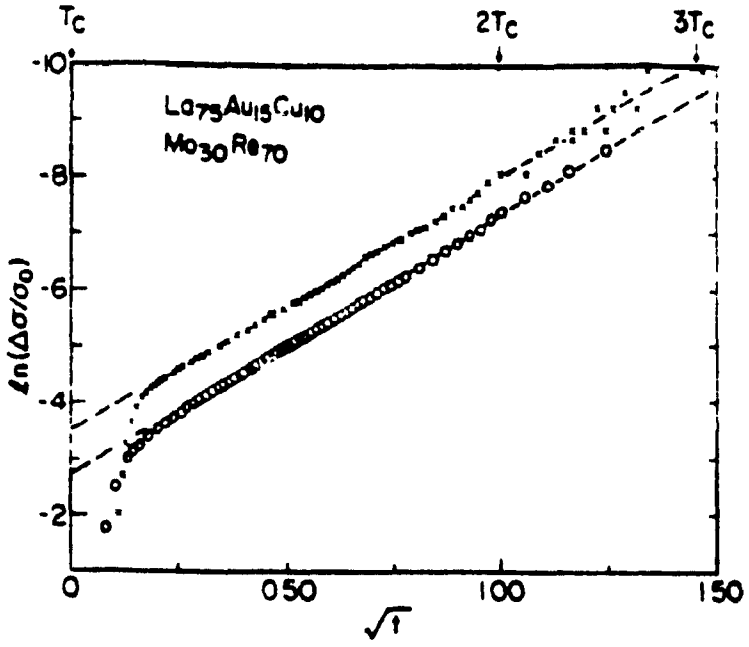


Figure 4.6: The logarithm of the normalized superconducting fluctuation conductivity in $La_{75}Au_{15}Cu_{10}$ and $Mo_{30}Re_{70}$ as a function of the square root of the reduced temperature taken from [10]

i.e. a constant value for $\gamma$ for all the alloys in this series.

We have isolated the superconducting fluctuation related conductivity of the superconducting alloys in this series by the following procedure. We fitted the resistance curve of $NiZr_2$ (which has zero spin fluctuation resistivity) in Figure 4.7 to a background function $-A\sqrt{T}+B$, describing the quantum corrections discussed in section 2, and extrapolated this background to lower temperatures, i.e. down to 4 K. By subtracting this background from the measured resistance change, we obtained the superconducting fluctuation resistivity. We find that in $NiZr_2$, as expected, the superconducting fluctuation resistivity does decay exponentially with $\sqrt{t}$ as shown in the Figure 4.8.

$$\frac{\Delta\rho}{\rho(4.2)} = -Ae^{-\gamma\sqrt{t}} \tag{4.5}$$

From the fit to the data, the value of the decay constant $\gamma$ is found to be 3.4. Which, as discussed above, is taken to be the same for all the other superconducting alloys. The superconducting related resistivity calculated for each of the alloys from equation (4.6), are subtracted from their measured resistivities.

After the corrections due to superconductivity, the resistivities of these alloys varied as $-A\sqrt{T}+B$ from the lowest available temperature till around 14K. In Figure 4.9, the resistivities of $Fe_{.5}Ni_{.5}Zr_2$ and $Fe_{.4}Ni_{.6}Zr_2$ are plotted against $\sqrt{T}$ in the temperature range 4K to 14K. We found that the variation of the coefficient of $\sqrt{T}$, A, with the Fe concentration (x) in the alloy, can be expressed by the following simple empirical relation:

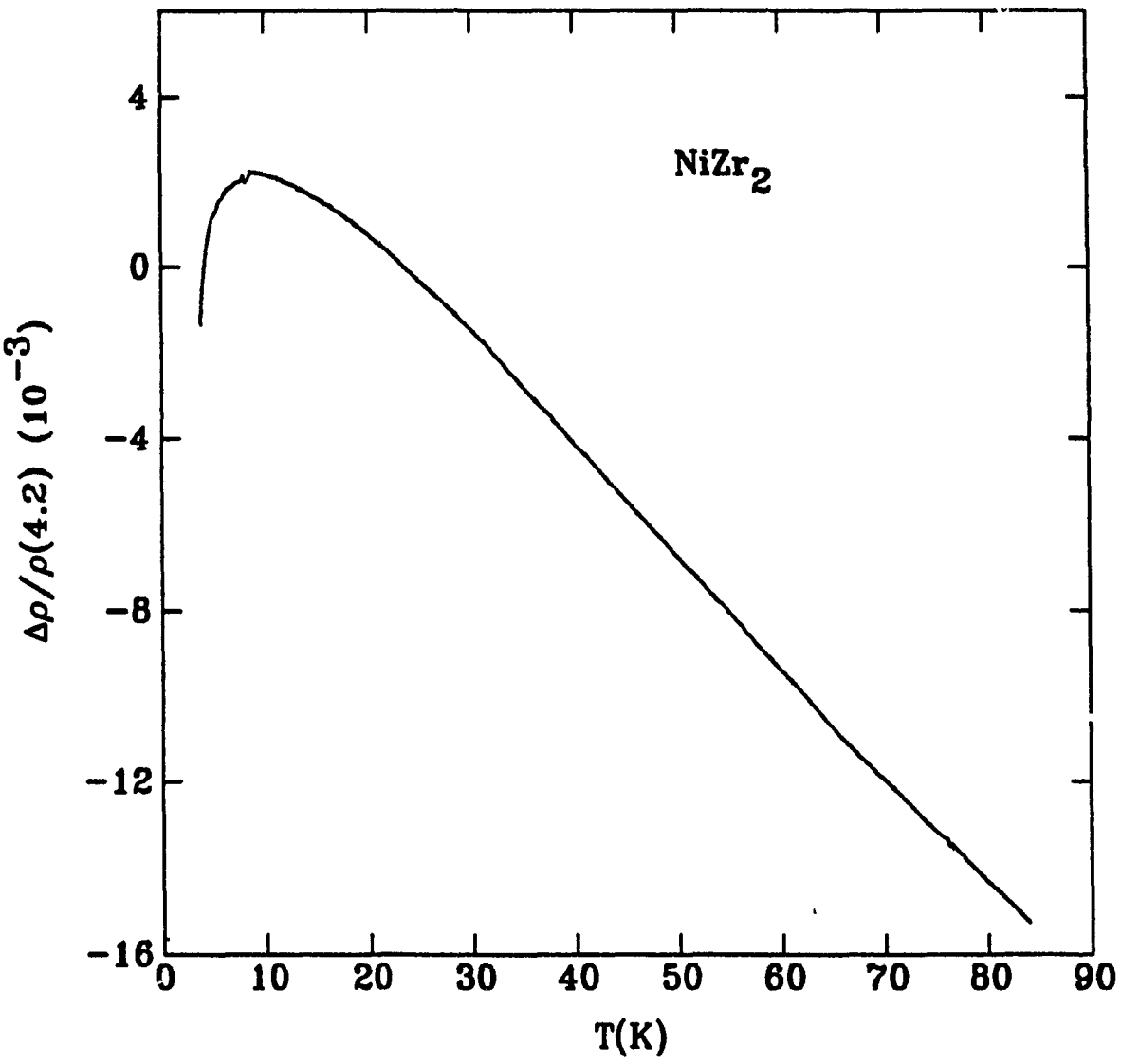


Figure 4.7: The resistivity of $NiZr_2$ as a function of temperature

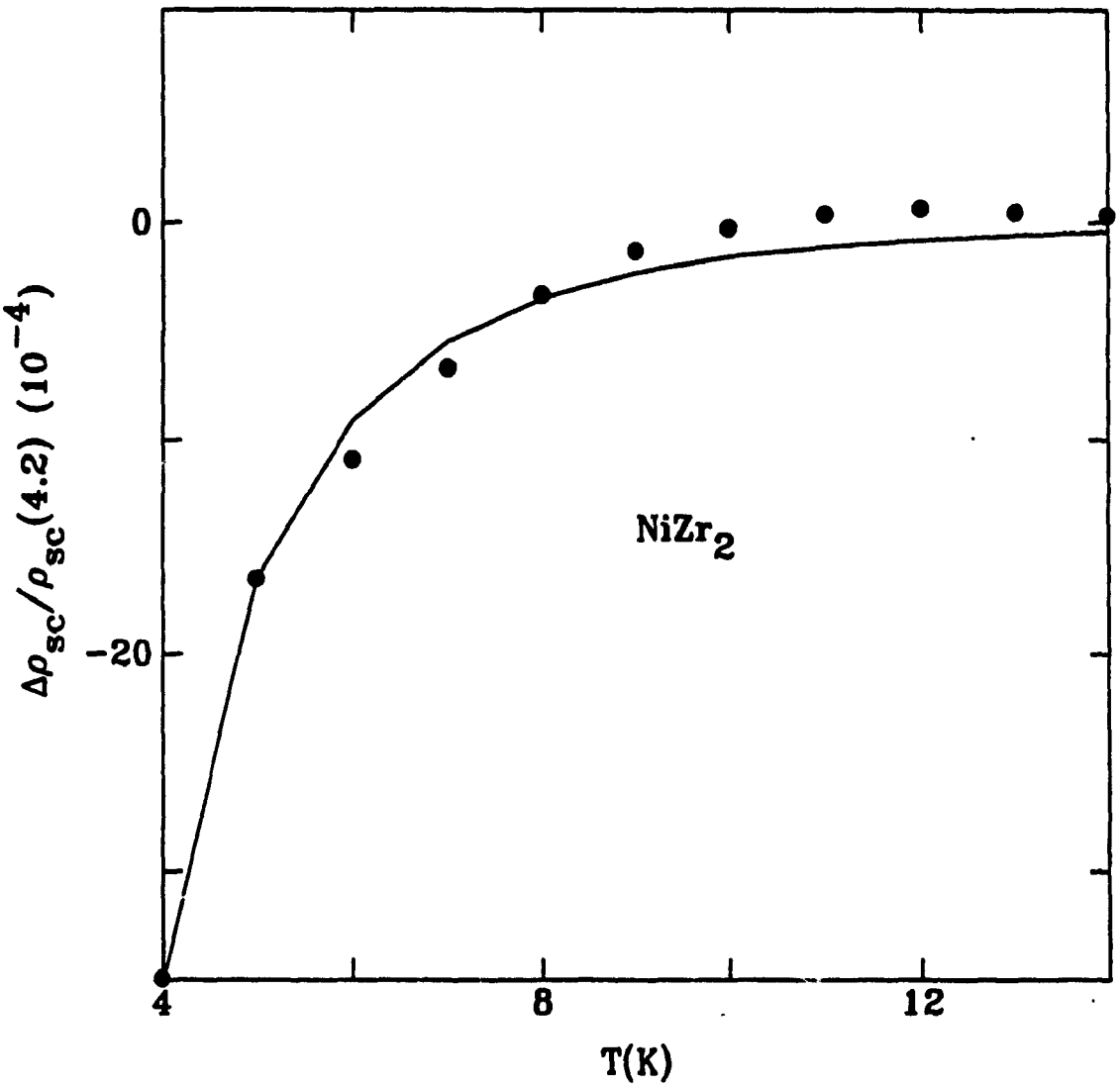


Figure 4.8: Normalized superconducting fluctuation resistivity of $NiZr_2$ as a function of temperature, the points are the experimental data and the solid line is a fit as described in the text [Eq. 4.5]

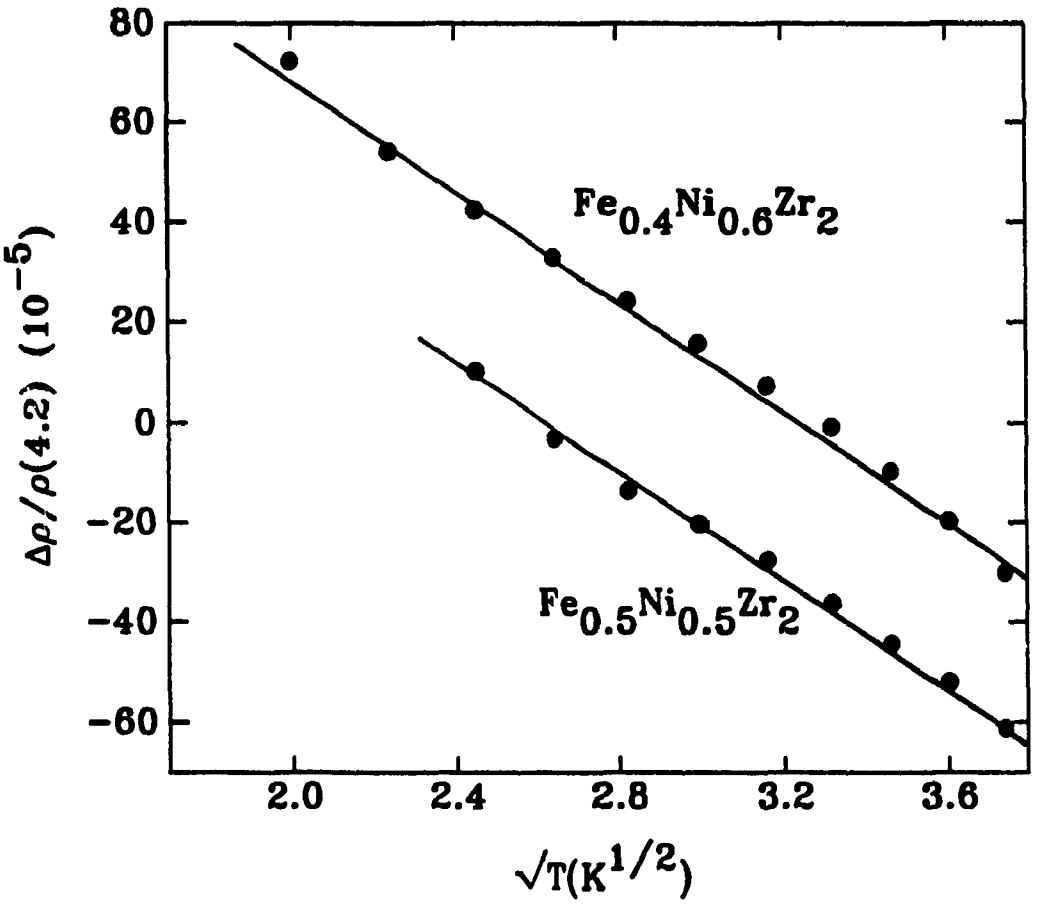


Figure 4.9: Normalized resistivities of $Fe_{0.4}Ni_{0.6}Zr_2$ and $Fe_{0.5}Ni_{0.5}Zr_2$ against the square root of the temperature.

$$A = 0.0018(1 - x)$$

where x is the Fe content. This is consistent with equation (4.3), since $T_c$ decreases with increasing Fe content.

## 4.4 Spin Fluctuation Resistivity

After the superconducting corrections, the large contribution due to spin fluctuations ($\rho_{sf}$) can finally be obtained for all compositions by subtracting off the resistivity of $NiZr_2$.

Using this procedure, we obtained $\rho_{sf}$ vs T curves, shown in Figure 4.10. The remarkable similarity of the shape of the curves strongly suggests a common origin for $\rho_{sf}$. These $\rho_{sf}$ vs T curves confirm the overall shape predicted for the local spin fluctuation resistivity component (given by Kaiser and Doniach as well as by Rivier and Zlatic [16], [21]), which varies as $T^2$ at low temperatures and changing to a linear dependence as T increases. Its size is comparable to that seen before in Fe-Zr system and in other crystalline systems.

Thus the unusual behaviour of resistivities of these alloys are due to the resistivity contribution from the spin fluctuations i.e. the scattering of conduction electrons from the $d$ band spin fluctuations. Kaiser and Doniach theory accounts for the experimental data on a wide variety of nearly magnetic systems including those with localized spin fluctuations as well as systems with uniform spin fluctuations.

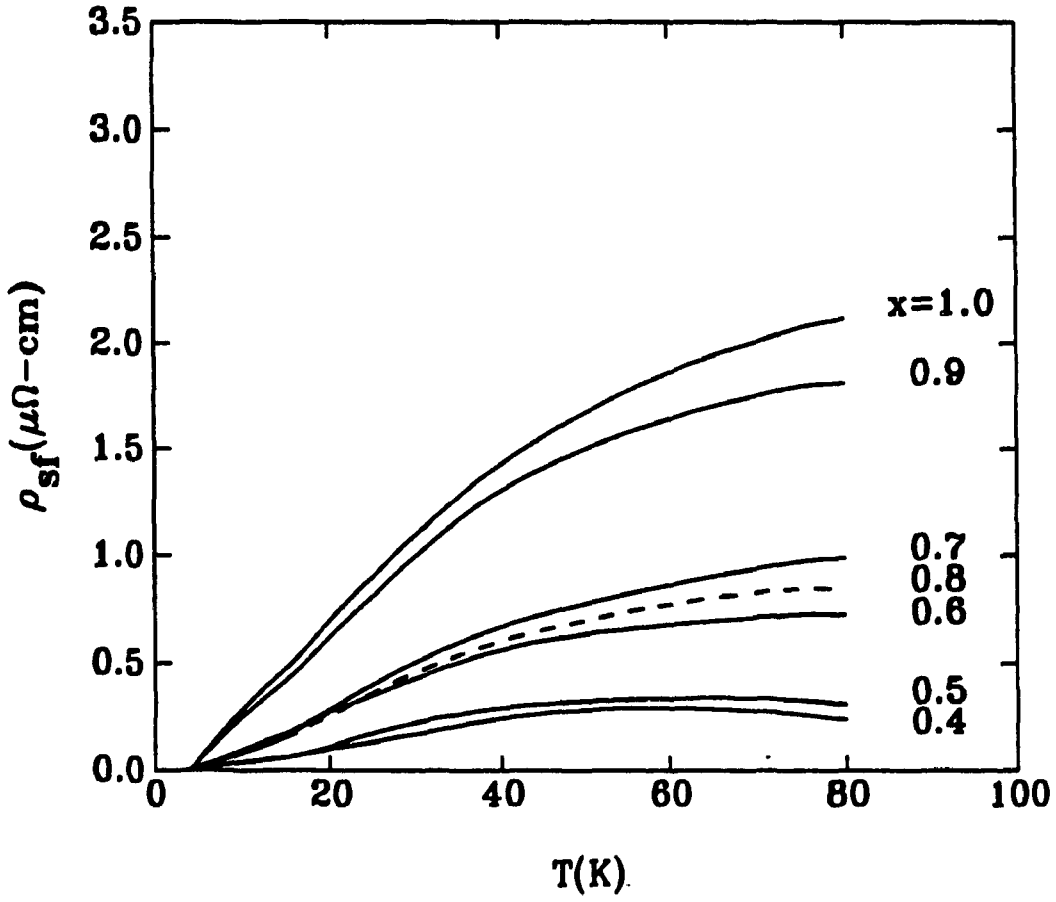


Figure 4.10: The spin fluctuation resistivity vs.temperature of $Fe_xNi_{1-x}Zr_2$ metallic glasses. As mentioned in section 3.3.3, for x = 0.8, the Zr content was higher than the nominal content

We have seen from Figure 4.10 that the characteristics of the measured spin fluctuation resistivity agree qualitatively with the predictions of Kaiser and Doniach's theory. We can now compare experimental data and theory quantitatively. In doing so we will determine the unknown parameters $\rho_{so}, T_{sf}$ and $\rho_0$. From the data shown in Figure 4.10, we find that spin fluctuation resistivity follows a $T^2$ behaviour up to 20 K. We, therefore, fit the data to the Kaiser and Doniach's expression which, at the low temperature limit ($T \rightarrow 0$) can be written as:

$$\rho_{sf} = \frac{\pi^2}{3}\left[\frac{T}{T_{sf}}\right]^2 \rho_{s0} - \rho_0 \tag{4.6}$$

$\rho_{so}, T_{sf}$ and $\rho_0$ are the fitting parameters. $\rho_{so}$ is the scaling factor, and $\rho_0$ is a small constant, needed because $\rho_{sf}(T)$ is, by our definition, zero at 4.2K rather than 0K. Now if we take the higher temperatures, i.e. above 20K, we can see the linear behaviour of the spin fluctuation resistivity. We were also able to fit the linear portion of the spin fluctuation resistivity above 20K, to the high temperature limit of $\rho_{sf}$ given by Kaiser and Doniach.

$$\frac{\rho_{sf}}{\rho_{s0}} = \frac{\pi}{2}\frac{T}{T_s} - \frac{1}{2} \tag{4.7}$$

The data are fitted by a multiparameter least-squares fitting routine. First, we start fitting with some initial values for $\rho_{so}, T_{sf}$ and $\rho_0$ and let them vary according to the fitting routine. The process stops when the deviation between the data and the theoretical expression is at a minimum. $\rho_{so}$ obtained from the linear fit was found to be a composition independent quantity. The values of $\rho_{so}$ for different compositions, had a scatter of less than 10%, whereas $T_{sf}$ increases with decreasing Fe content as

expected. To obtain an internally consistent fit, $\rho_{so}$ was fixed to its average value and the analysis repeated with $T_{sf}$ being the main adjustable parameter. Our analysis therefore yields a well defined value of spin fluctuation temperature $T_{sf}$.

Figure 4.11 shows the low temperature fitting of the data for different compositions. For the compositions $FeZr_2$ and $Fe_{0.9}Ni_{0.1}Zr_2$, we could not see the $T^2$ behaviour down to 4 K. This is because, the spin fluctuation temperatures of these alloys are very low, so that $T^2$ law occurs below the temperature range observed here. The theory predicts that the temperature dependence changes gradually from $T^2$ to T at temperatures of the order of $0.25T_{sf}$. For the alloys studied here, the power law of spin fluctuation resistivity at the lowest temperatures is found to be consistent with 2, but not $\frac{3}{2}$ as suggested by Riseborough [32]. Within the error, the values of $T_{sf}$ for different compositions obtained from the T fit are consistent with those calculated from the $T^2$ fit.

We finally fitted the data in the entire temperature range from 4K to 80K, to the full analytical expression given by Kaiser and Doniach for the spin fluctuation resistivity, equation (2.8). Fig 4.12 shows the experimental data of spin fluctuation resistivity and the solid line is the fit as explained above. The resulting spin fluctuation temperature $T_{sf}$ increases with the decreasing Fe content, i.e. as we move away from the magnetic transition. $T_{sf}$ is plotted against the composition in Fig 4.13.

It may be seen that after the corrections of the superconductivity, the agreement between the theory and the experiment is excellent up to the temperature

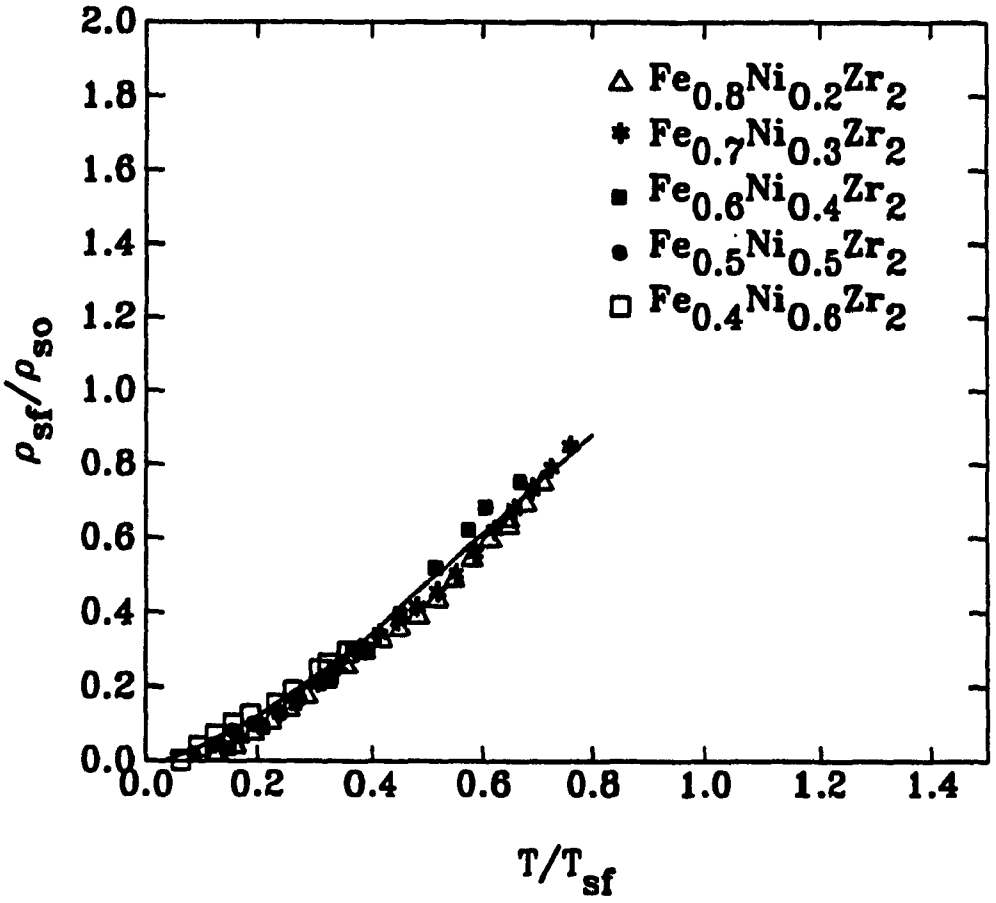


Figure 4.11: The low temperature spin fluctuation resistivity of five $Fe_xNi_{1-x}Zr_2$ alloys fitted to the expression of Kaiser and Doniach [Eq. (4.6)]

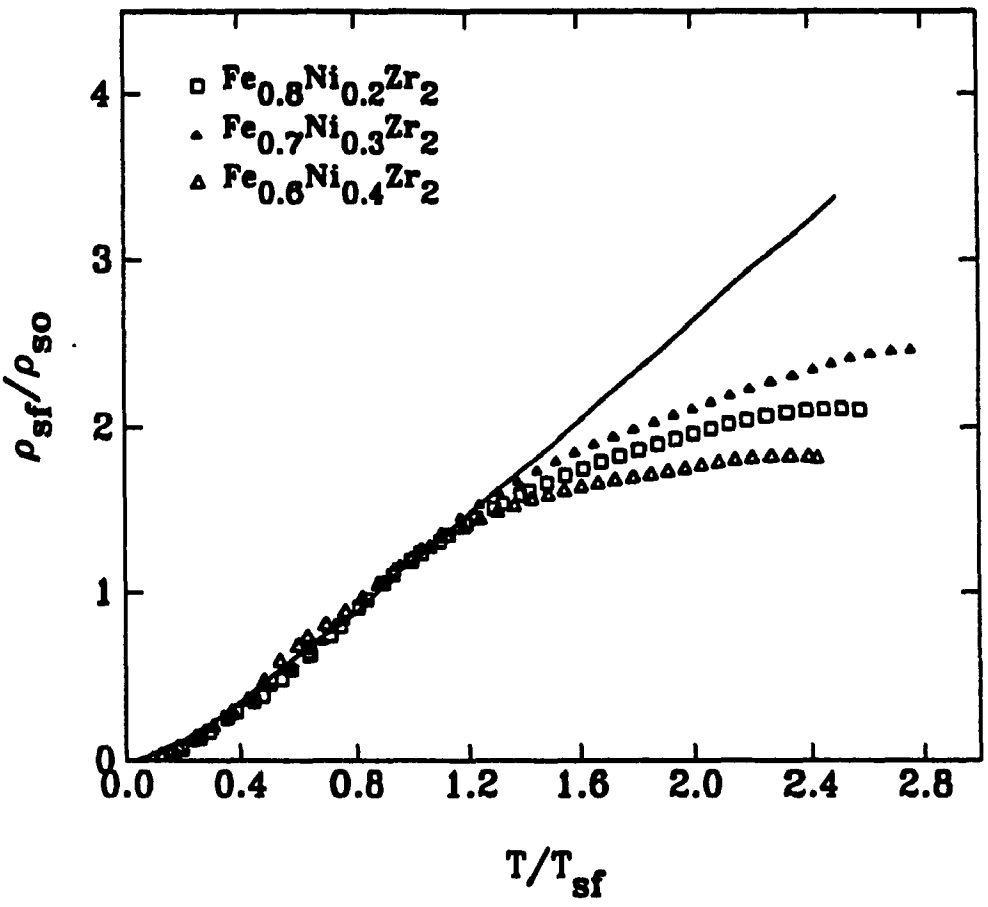


Figure 4.12: Spin fluctuation resistivities of $Fe_{0.8}Ni_{0.2}Zr_2$, $Fe_{0.7}Ni_{0.3}Zr_2$ and $Fe_{0.6}Ni_{0.4}Zr_2$. Solid line is a fit as described in the text [Eq. (2.8)].

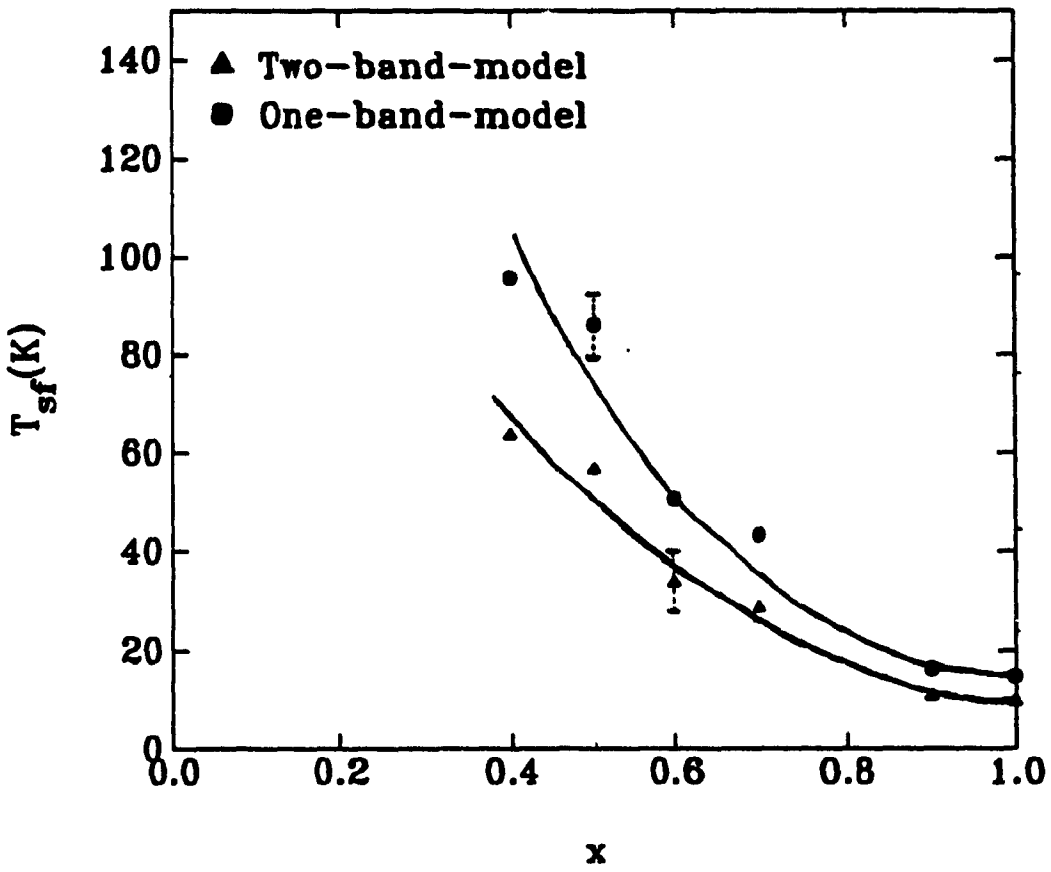


Figure 4.13: The spin fluctuation temperatures of $Fe_xNi_{1-x}Zr_2$ metallic glasses obtained by one band and two band models.The solid lines are a guide to the eye.Error bars are shown for both models.

40 K. Moreover it is equally good for all the compositions. Therefore we conclude that the spin fluctuation theory suggested by Kaiser and Doniach for the crystalline systems, describes the observed anomaly well in the amorphous systems also , for temperatures $\leq T_{sf}$.

However, the theory of Kaiser and Doniach predicts a fall-off in resistivity below the linear law at higher temperatures, caused by the temperature dependence of the spectral density. This fall-off increases with the increasing local enhancement $\alpha$. For the alloys studied here, the local enhancement is very small i.e. of order 7 [13], and is not expected to show a marked difference from the linear law. Our experimental results, however, showed significant deviation below the linear law at higher temperatures, which is not expected according to the theory.

The predictions that the resistivity due to the scattering of conduction electrons by spin fluctuations, increases as $T^2$ and then as T, by Kaiser and Doniach, had been confirmed by many other researchers, for example, Rivier and Zlatic [21]. Rusby [43] and Laborde and Radhakrishna [44].

However, according to Rivier and Zlatic, the concave nature of the spin fluctuation resistivity at higher temperatures, comes naturally from the theory. The characteristic fall-off marks the onset of the logarithmic regime. The spin fluctuation temperatures obtained with Rivier and Zlatic's model, are plotted in Figure 4.13 along with those obtained by Kaiser and Doniach's model for each composition. The spin fluctuation temperatures for different alloys obtained from both one band and two band models are given in table 4.2. Values of $T_{sf}$ calculated from Kaiser and

Doniach model are about 30 % smaller than those of the Rivier and Zlatic model.

| *Composition* | $T_{sf}$ *(K)* | |
|---|---|---|
| | *Two band Theory* | *One band Theory* |
| $FeZr_2$ | 10 | 15 |
| $Fe_{0.9}Ni_{0.1}Zr_2$ | 11 | 16.5 |
| $Fe_{0.8}Ni_{0.2}Zr_2$ | 30 | 46.4 |
| $Fe_{0.7}Ni_{0.3}Zr_2$ | 29 | 43.6 |
| $Fe_{0.6}Ni_{0.4}Zr_2$ | 34 | 51 |
| $Fe_{0.5}Ni_{0.5}Zr_2$ | 57 | 86.5 |
| $Fe_{0.4}Ni_{0.6}Zr_2$ | 64 | 96 |

Table 4.3: Spin fluctuation temperatures obtained from two band and one band models.

# Chapter 5

# Conclusions

We have presented the measurements of temperature dependent resistivities of fourteen different Fe-Ni-Zr metallic glasses. The major contribution to the resistivity in amorphous alloys, i.e. the contribution due to its structure, is constant across the alloy series studied here. Hence, the procedure used in this work to extract the spin fluctuation resistivity is straightforward and allows, for the first time, qualitative and quantitative analysis of the effects of spin fluctuations on the resistivity in amorphous alloys. Our analysis confirm the qualitative results of preliminary work done in this type of nearly magnetic alloys [12]. A complete description of the experimental data at low temperature is given in terms of superconductivity, quantum corrections and spin fluctuation contributions. Our principal success is the verification of the validity of the one band and two band models of spin fluctuations.

The superconducting fluctuation resistivity in the alloys of $Fe_xNi_{1-x}Zr_2$ system, was isolated. In these alloys, the superconducting fluctuation resistivity is

found to decay as $exp(-\gamma\sqrt{t})$ with the reduced temperature $t = \frac{T-T_c}{T_c}$, in agreement with the experimental results of Johnson et al. [10], $\gamma$ is 3.4 for our alloys. For alloys containing less than 20 atomic % Fe, the quantum corrections to the resistivity have to be taken into account below 14K. In this region, the resistivity varies as $-A\sqrt{T}$. The value of A was found to increase with decreasing Fe content in the samples.

The procedure used here to extract the spin fluctuation resistivity is more accurate than the methods used in the previous experiments [e.g. [12], [26]]. The spin fluctuation resistivity varies as $T^2$ at lowest temperatures and as T at higher temperatures, which is consistent with the two band model of Kaiser and Doniach and the one model suggested by Rivier and Zlatic [21]. The significant fall-off of the resistivity at further higher temperatures, below the linear law, is not as predicted by Kaiser and Doniach. On the other hand the one band model of Rivier and Zlatic seems to explain this behaviour well. The spin fluctuation temperature calculated from the above models, is minimum when the system is close to the magnetic transition and increases as the system moves away from the magnetic transition.

Suggestions for the further work are: To analyse the effect of external magnetic field on the spin fluctuation resistivity and extending the resistivity measurements up to room temperature to study the high temperature plateau of the spin fluctuation resistivity. The effects of spin fluctuations on other transport properties such as thermopower and Hall effect should also be investigated.

# References


[1] P.J. Cote and L.V. Meisel, "Electrical transport in glassy metals" in *Glassy Metals I* , edited by H.-J.Guntherodt and H.Beck (Springer-Verlag Berlin Heidelberg, New York, 1981).

[2] E. Abrahams, P.W. Anderson, D.C. Licciardello and T.V. Ramakrishnan, Phys. Rev. Lett. **42**, 673 (1979).

[3] B.L. Altshuler and A.G. Aronov, in *Electron-Electron interaction in Disordered systems*, edited by A. L. Efros and M. Pollak (North-Holland, Amsterdam, 1985).

[4] P.A. Lee and T.V. Ramakrishnan, Rev. Mod. Phys. **57**, 287 (1985).

[5] G. Bergmann, Phys. Rep **107**, 1 (1984).

[6] A. Sahnoune and J.O. Strom-Olsen, Phys. Rev. B **39**, 7561 (1989).

[7] L.G. Aslamasov and A.I. Larkin, Phys. Lett. **A26**, 238 (1968).

[8] S. Ami and K. Maki, Phys. Rev. **B18**, 4714 (1978).

[9] S. Ami and K. Maki, Phys. Rev. **B19**, 1403 (1979).

[10] W.L. Johnson and C.C. Tsuei, Phys. Rev. **B13**, 4827 (1976).

[11] W.L. Johnson, C.C. Tsuei and P. Chaudhari, Phys. Rev. **B17**, 2884 (1978).

[12] J.O. Strom-Olsen, Z. Altounian, R.W. Cochrane and A.B. Kaiser, Phys. Rev. B **31**, 6116 (1985).

[13] E. Batalla, Z. Altounian and J.O. Strom-Olsen, Phys. Rev. B **31**, 577 (1985).

[14] B.R. Coles, Phys. Lett. **8**, 243 (1964).

[15] P. Lederer and D.L. Mills, Phys. Rev. **165**, 837 (1968).

[16] A.B. Kaiser and S. Doniach, Intern. J. Magnetism **1**, 11 (1970).

[17] D. Greig and J.A. Rowlands, J. Phys. F **4**, 232 (1974).

[18] G.S. Knapp and M.P. Sarachik, J. Appl. Phys. **40**, 1474 (1969).

[19] G.S. Knapp, J. Appl. Phys. **38**, 1267 (1967).

[20] M.P. Sarachik, Phys. Rev. **170**, 679 (1968).

[21] N. Rivier and V. Zlatic, J. Phys. F:Metal Phys. **2**, L99 (1972).

[22] W.L. Johnson, S.J. Poon and P. Duwez, Phys. Rev. B **11**, 150 (1975).

[23] Z. Altounian and J.O. Strom-Olsen, Phys. Rev. B **27**, 4149 (1983).

[24] Z. Altounian, C.A. Volkert and J.O. Strom-Olsen, J. Appl. Phys. **57**, 1777 (1985).

[25] P.A. Wolff, Phys. Rev. **124**, 1030 (1961).

[26] R. Jullien, M.T. Beal-Monod and B. Coqblin, Phys. Rev. B **9**, 1441 (1974).

[27] D.L. Mills and P. Lederer, J. Phys. Chem. Solids **27**, 1805 (1966).

[28] A.B. Kaiser, Aust. J. Phys. **36**, 537 (1983).

[29] A.I. Schindler and M.J Rice, Phys. Rev. **164**, 759 (1967).

[30] L.S. Cheng, R.J. Higgins, J.E. Graebner and J.J. Rubin, Phys. Rev. B **19**, 3722 (1979).

[31] K.H. Fisher, J. Low Temp. Phys. **17**, 87 (1974).

[32] S. Peter Riseborough, Phys. Rev. B **29**, 4134 (1984).

[33] R. Reinhart, Ph.D. thesis, McGill University, Montreal, Canada, 1988.

[34] Z. Altounian, T. Guo-hua and J.O. Strom-Olsen, J. Appl. Phys. **54**, 3111 (1983).

[35] W.B. Muir and J.O. Strom-Olsen, J. Phys. E : Sci. Instrum **9**, 163 (1976).

[36] R.W. Cochrane, B.J. Kastner and W.B. Muir, J. Phys. E : Sci. Instrum. **15**, 425 (1982).

[37] B.J. Hickey, D. Greig and M.A. Howson, J. Phys. F : Met. Phys. **16**, L13 (1986).

[38] A. Sahnoune, M.Sc. thesis, McGill University, Montreal, Canada, 1988.

[39] J.O. Strom-olsen, "The electron transport properties of amorphous metals" in *Amorphous metals*, edited by Henryk Matyja, Piotr G. Zielinski (World scientific publishing co. pte. ltd., 242, Cherry street, Philadelphia, USA, 1985).

[40] M. Olivier, J.O. Strom-Olsen, Z. Altounian and R.W. Cochrane, in *Proc. LITPIM Supp.*55, (PTB Braunschwieg, West Germany, 1984).

[41] J.B. Bieri, A. Fert, G. Creuzet and J.C. Ousset, Solid state Communications **49**, 849 (1984).

[42] S.J. Poon, K.M. Wong and A.J. Drehman, Phys. Rev. **B31**, (1985).

[43] R. Rusby, J. Phys. F **4**, 1265 (1974).

[44] O. Laborde and P. Radhakrishna, Phys. Lett. **37A**, 209 (1971).